Sun *et al. Energy Mater* 2024;4:400027
DOI: 10.20517/energymater.2023.88

Energy Materials

Review

Open Access

Check for updates

Recent advances in nanoscale engineering of Pd-based electrocatalysts for selective CO_2 electroreduction to formic acid/formate

Shangqing Sun[1,#], Yalan Mao[1,#], Fang Liu[1], Shukang Zhang[1], Yidan Sun[1], Qiang Gao[2], Xiaojing Liu[1,*]

[1]State Key Laboratory of Materials-Oriented Chemical Engineering, School of Energy Science and Engineering, College of Chemical Engineering, Nanjing Tech University, Nanjing 211816, Jiangsu, China.
[2]Department of Chemistry, University of Virginia, Charlottesville, VA 22904, USA.
[#]Authors contributed equally.

***Correspondence to:** Dr. Xiaojing Liu, State Key Laboratory of Materials-Oriented Chemical Engineering, School of Energy Science and Engineering, Nanjing Tech University, 30 South Puzhu Road, Nanjing 211816, Jiangsu, China. E-mail: xjliu022@njtech.edu.cn

How to cite this article: Sun S, Mao Y, Liu F, Zhang S, Sun Y, Gao Q, Liu X. Recent advances in nanoscale engineering of Pd-based electrocatalysts for selective CO_2 electroreduction to formic acid/formate. *Energy Mater* 2024;4:400027. https://dx.doi.org/10.20517/energymater.2023.88

Received: 2 Nov 2023 **First Decision:** 9 Jan 2024 **Revised:** 22 Jan 2024 **Accepted:** 5 Mar 2024 **Published:** 26 Mar 2024

Academic Editor: Hao Liu **Copy Editor:** Fangyuan Liu **Production Editor:** Fangyuan Liu

Abstract

Electrochemical conversion of carbon dioxide (CO_2) into high-value chemicals and fuels driven by electricity derived from renewable energy has been recognized as a promising strategy to achieve carbon neutrality and create sustainable energy. Particularly from the viewpoint of the product values and the economic viability, selective CO_2 reduction to formic acid/formate has shown great promise. Palladium (Pd) has been demonstrated as the only metal that can produce formic acid/formate perfectly near the equilibrium potential; yet, it still suffers from CO poisoning, poor stability and competitive CO pathway at high overpotentials. Herein, recent progress of Pd-based electrocatalysts for selective CO_2 electroreduction and their mechanistic understanding are reviewed. First, the fundamentals of electrochemical CO_2 reduction and the reaction pathway of formic acid/formate on Pd are presented. Then, recent advances in the rational design and nanoscale engineering strategies of Pd-based electrocatalysts for further improving CO_2 reduction activity and selectivity to formic acid/formate product, including size control, morphology and shape control, alloying, heteroatom doping, surface-strain engineering, and phase control, are discussed from the perspectives of both experimental and computational aspects. Finally, we discuss the pertinent challenges and describe the future prospects and opportunities in terms of the development of electrocatalysts, electrolyzers and characterization techniques in this research field.

Keywords: Electrochemical CO_2 reduction, formic acid/formate, Pd-based catalysts, nanoscale engineering, electrocatalysis

INTRODUCTION

Fossil fuels such as coal, crude oil, and natural gas are primarily responsible for the world's rapid economic development, industrial output and human activities. However, extensive consumption of fossil fuels and the associated carbon dioxide (CO_2) emissions into atmosphere lead to energy crisis and global environmental issues worldwide[1-3]. According to recent studies and data, the CO_2 atmospheric concentration increased to 420.41 ppm in 2023, a rapid rise from 340 ppm in 1980 (by 80.41 ppm), with an alarming yearly average rate of 2.47 ppm[4]. It is essential to develop renewable energy sources and CO_2 conversion technologies in order to reduce CO_2 emissions and obtain carbon neutrality. As a result, four categories of efficient solutions-carbon reduction, carbon capture, carbon utilization, and carbon sequestration-are essential[4-7]. Taking into account the accumulated CO_2 and urgent demand of renewable energy, the conversion of CO_2 into valuable resources, which enables it to re-enter the social carbon cycle system, is a crucial step in achieving carbon neutrality[8-10].

CO_2 conversion technologies, such as biochemical conversion, thermochemical conversion, photochemical reduction and electrochemical reduction, have emerged as promising responses to the aforementioned issues in recent years[11,12]. Due to its benefits of moderate reaction conditions, adjustable product selectivity and great potential for practical applications, electrochemical CO_2 reduction reaction (ECO_2RR) driven by energetic electrons, in particular, gained considerable research interest. Such technology drives the conversion of waste into sustainable fuels and chemicals using renewable electricity from solar and wind energy[13]. Importantly, ECO_2RR offers a promising strategy to close the anthropic carbon cycle and achieve sustained carbon neutralization since it not only decreases CO_2 accumulation but also enhances energy storage in the form of chemical bonding of high-energy-density carbonaceous chemicals[14,15].

In electrocatalytic CO_2 reduction reaction (CO_2RR) systems, renewable electricity powered electrocatalysis could convert CO_2 into several C_1-C_3 products, including formic acid (HCOOH)/formate ($HCOO^-$)[16,17], carbon oxide (CO)[18], methane (CH_4)[19], ethanol (CH_3CH_2OH)[20], ethylene (C_2H_4)[21], acetic acid (CH_3COOH)[22,23], n-propanol ($CH_3CH_2CH_2OH$)[24], *etc.* Of these reaction products, formic acid, in particular, is a highly valuable liquid product and an important platform chemical in a variety of industries, such as pharmaceuticals, metallurgical, and leather industries. Notably, formate can be neutralized *in situ* to easily yield formic acid. Formic acid is also regarded as a convenient and prospective hydrogen storage medium, which serves as a green energy source for direct formic acid fuel cells due to its advantages of non-toxicity, in-situ hydrogen supply and high hydrogen density[2,25,26]. Therefore, it is quite appealing to produce formic acid/formate by directly utilizing CO_2. Given that the cost of operating a CO_2 electrolyzer is highly dependent on the price of electricity, formic acid/formate exhibits a much higher added value and is more economically viable than other C_2-C_4 products[25,27-29]. Focusing on formic acid/formate produced by CO_2 electroreduction has shown great promise from an economic standpoint. It is crucial to design sophisticated catalysts with superior catalytic performance given the ongoing development of ECO_2RR and the rising demand for formic acid/formate products. Main-group p-block metals, such as indium (In)[30], tin (Sn)[31], and bismuth (Bi)[16], have been reported to exhibit exclusive selectivity toward formic acid/formate[25,32]. Even though enormous progress has been made in achieving high Faraday efficiency (FE), it is still challenging to produce formic acid/formate with a high overall energy efficiency because the reactions have sluggish kinetics and high overpotentials on main-group p-block metals. Palladium (Pd), as a member of the platinum group metals, possesses a unique $4d^{10}5s^0$ electronic structure and demonstrates exceptional performance in a variety of catalytic reactions, including CO_2 electroreduction[33,34], formic acid oxidation[35], methane catalytic combustion[36], and CO oxidation[37]. When acting as an electrocatalyst for ECO_2RR, Pd is

unique because it is the only metal that can electrochemically reduce CO_2 to formic acid/formate at a near-zero overpotential[38-40]. This means that Pd can select highly for CO_2 reduction products even under conditions similar to those of the hydrogen evolution reaction (HER) in an aqueous system[41]. However, considerable obstacles in practical applications remain to be overcome. Since the electrocatalyst significantly affects the performance of the ECO_2RR, developing active and selective electrocatalysts for certain products is the main focus for research of this field.

In this review, we highlight recent progress in the nanoscale of Pd-based catalysts for converting CO_2 to formic acid/formate. The review starts with the formic acid/formate generation reaction mechanism on Pd catalyst. Then, various engineering strategies of nanostructured Pd-based electrocatalysts for selective CO_2 reduction to formic acid/formate are summarized. Finally, we conclude by discussing the pertinent challenges and providing an overview of the future prospects and opportunities for developing high-performance electrocatalysts and the appropriate reactors for producing formic acid/formate.

Fundamental ECO_2RR mechanisms of Pd electrocatalysts

The CO_2 molecule is chemically inert and thermodynamically relatively stable[42], so activating it on the catalyst surface needs a high activation energy which must be overcome by applying a much negative reduction potential[43]. In an aqueous solution with a pH value of 7.0, the thermodynamic potential for the first electron transfer of CO_2 to form CO^{2-} is -1.90 V (*vs.* standard hydrogen electrode, SHE), which is adverse for the reaction[44-46]. In contrast, proton-assisted multiple electron transfer processes can occur at lower negative potentials (-0.2~-0.6 V *vs.* SHE) on appropriate catalyst surfaces, which helps to stabilize reaction intermediates and subsequently leads to the formation of various CO_2 derivatives[47].

As shown in Figure 1A, ECO_2RR, a complicated process[48], contains multielectron and proton coupling steps, involving 2 to 12 electron reaction pathways [Figure 1B][49] and generating various reduction products[50]. In general, the multi-step reaction includes three main steps: (1) CO_2 chemisorption and activation on the catalyst surface. This step involves the first electron transfer from the catalyst to CO_2 to form $*CO_2^{\bullet-}$ (*infers the adsorption site), along with the proton transfer from the electrolyte, forming *COOH or *OCHO. The *COOH or *OCHO intermediate is immediately stabilized on the metal surface by forming a metal-carbon or metal-oxygen bond; (2) Electron transfer from electrocatalyst to *COOH or *OCHO on the metal surface is accompanied by the proton transfer from the electrolyte, resulting in the formation of adsorbed key intermediates and their eventual product; and (3) Desorption of the products from the electrocatalyst surface and diffusion into the electrolyte[5].

The vast majority of ECO_2RR electrocatalysts studied at this stage are mainly based on various metal-based materials[19,51-53]. The type and yield of the targeted product is controlled by tuning the binding ability of their surface and the adsorbed intermediates (*CO, *COOH, *CHO, *COH)[54-57]. For example, for the C1 products, when the interaction between the electrocatalyst surface and the intermediates is not strong enough, $HCOOH/HCOO^-$ and CO are the main reduction products [Figure 2]. As schematically illustrated in Figure 2, different adsorption configurations of $*CO_2^{\bullet-}$ radical anion on the electrode surface usually determine the final formation of $HCOOH/HCOO^-$ or CO product. In brief, if O atoms in $*CO_2^{\bullet-}$ act as the binding sites via an oxygen coordination mode, the carbon atom in $*CO_2^{\bullet-}$ is protonated to create *OCHO, which is further reduced to $HCOO^-$ after electron transfer[58]. This is because the C-O bond cannot be dissociated in the case of weak interaction[59]. The final liquid C1 product in the electrolyte can exist in the form of either formic acid or formate, which depends on the pH of the electrolyte. Alternatively, when the adsorption configuration is carbon coordination mode, $*CO_2^{\bullet-}$ binds on the electrode surface through the carbon atom, and the oxygen atom in $*CO_2^{\bullet-}$ radical intermediate is protonated to generate the carboxyl

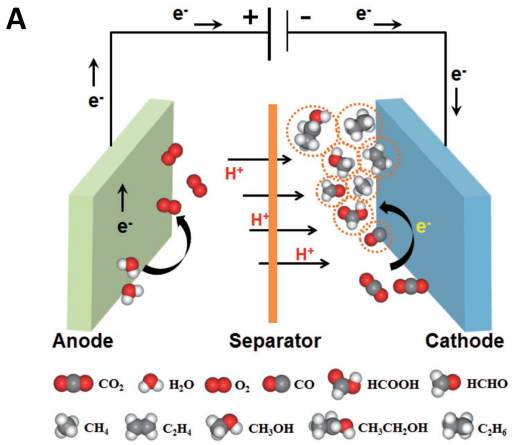

B

Product	Chemical reaction	Equilibrium standard potential, E^0 (V vs. RHE)
CO	$CO_2 + 2e^- + 2H^+ \rightleftharpoons CO\ (g) + H_2O$	−0.10
HCOOH	$CO_2 + 2e^- + 2H^+ \rightleftharpoons HCOOH\ (aq)$	−0.2
CH_3OH	$CO_2 + 6e^- + 6H^+ \rightleftharpoons CH_3OH\ (aq) + H_2O$	0.10
CH_4	$CO_2 + 8e^- + 8H^+ \rightleftharpoons CH_4\ (g) + 2H_2O$	0.03
CH_3COOH	$2CO_2 + 8e^- + 8H^+ \rightleftharpoons CH_3COOH\ (aq) + 2H_2O$	−0.26
CH_3COH	$2CO_2 + 10e^- + 10H^+ \rightleftharpoons CH_3CHO\ (aq) + 3H_2O$	0.05
CH_2CH_2	$2CO_2 + 12e^- + 12H^+ \rightleftharpoons CH_2CH_2\ (g) + 4H_2O$	0.08
CH_3CH_2OH	$2CO_2 + 12e^- + 12H^+ \rightleftharpoons CH_3CH_2OH\ (aq) + 3H_2O$	0.09
$CH_3CH_2CH_2OH$	$3CO_2 + 18e^- + 18H^+ \rightleftharpoons CH_3CH_2CH_2OH\ (aq) + 5H_2O$	0.21
H_2	$2H^+ + 2e^- \rightleftharpoons H_2\ (g)$	0.00
O_2	$2H_2O \rightleftharpoons O_2\ (g) + 4H^+ + 4e^-$	1.23

Figure 1. (A) Illustration of the electrochemical CO_2 reduction process and the possible products generated in the CO_2 electrolyzer[48]. Reprinted with permission. Copyright 2018, WILEY[48]. (B) The reduction potentials of the semi-reactions of the most commonly ECO_2 RR products in aqueous media (pH 7, 1 atm and 25 °C, 1 M solute concentration)[49]. Reprinted with permission. Copyright 2023, WILEY[49].

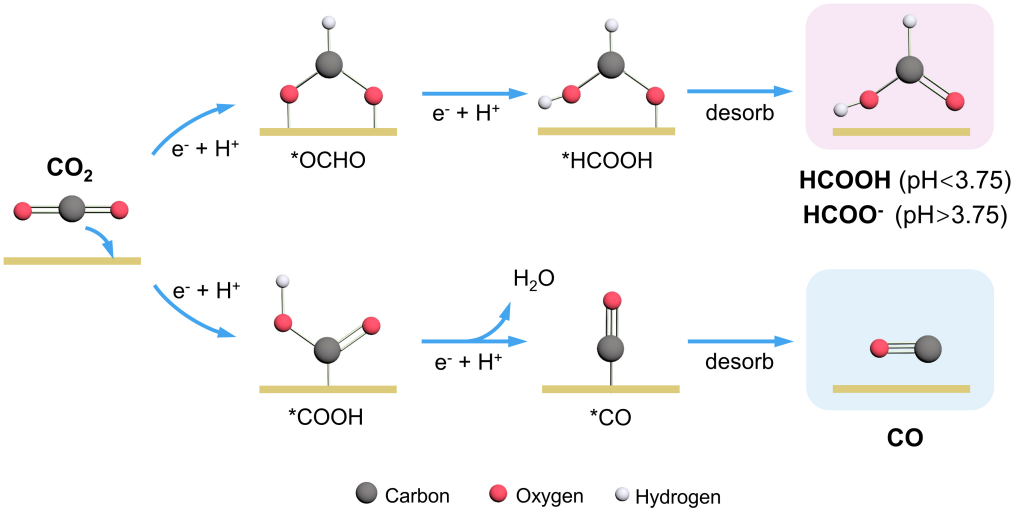

Figure 2. Schematic diagram of proposed reaction pathways of electrochemical reduction CO_2 to HCOOH/ $HCOO^-$ or CO product by forming different intermediates. (C atoms: black; O atoms: red; H atoms: white).

intermediate (*COOH), which is suggested as a key intermediate. *COOH is then reduced to *CO and desorbs from the electrode surface to generate CO product[27,60]. However, when the interaction of *CO is strong, the intermediates will undergo a more complicated process, accompanied by more electron transfer and protonation, leading to the formation of different types of hydrocarbon and alcohols[29,61,62].

For CO_2-to-HCOOH conversion, metal Pd has received great consideration and is recognized as a promising catalyst due to its high selectivity at low overpotentials[38,63]. Typically, Pd catalysts initially participate in ECO_2RR by preferentially adsorbing *H on the surface, forming an active hydrogen-adsorbed Pd surface (PdH_x phase)[39]. The relationship between the active-phase transformation and the formate

selectivity is highly associated with the applied potentials. As shown in Figure 3A, during the electrocatalytic reaction, the transformation from a pure hydrogen-absorbed PdH_x surface (above -0.2 V) to an almost bare metallic Pd surface (below -0.5 V) indicates a gradual decline in surface H coverage, which is controlled by the potentials and intermediates [Figure 3B]. At low potentials (> -0.2 V *vs.* reversible hydrogen electrode, RHE), the formation of a mixture of the α- and β-phases of a palladium-hydride core (α + β PdH_x@PdH_x) facilitates the *OCHO intermediates, favoring the production of formate. In the moderate potential range (-0.25~-0.45 V *vs.* RHE), the α + β PdH_x@PdH_x phase gradually transforms into the β-PdH_x@Pd phase. In this process, most of the surface PdH_x is covered by *CO intermediates and the number of active sites for *OCHO reduces, resulting in the formate pathway being suppressed and the competitive HER dominated. With the negative shift of bias voltage, the adsorbed *H gradually dissociates from the surface and destroys the initial mixed active phase. In the high potential region (< -0.45 V *vs.* RHE), the finally formed β-PdH_x phase selectively converts CO_2 into CO via *COOH intermediates dominated pathway, and CO subsequently dissociates and desorbs from the surface. In addition, the *CO intermediates coverage on the surface gradually increases as the potential shifts negatively, which makes the formation of PdH_x phases more favorable energetically, weakening the CO adsorption on the surface[63]. This phenomenon further explains the high CO selectivity at high overpotentials on Pd nanoparticles (NPs).

In short, these studies provide important insights into the catalytic mechanism of Pd NPs in ECO_2RR. In order to obtain stable formic acid/formate generation during the ECO_2RR process, the design of efficient Pd-based catalysts focuses mainly on two aspects: (1) adjusting the surface oxygen affinity of catalyst to preferentially adsorb *OCHO rather than *COOH; and (2) appropriately tuning the electronic structure to weaken the binding strength of *CO at surface active sites. Next, several nanoscale design strategies for improving the ECO_2RR performance of Pd-based electrocatalysts and an exposition of their recent advancements are outlined. Therefore, it is worthwhile to start reviewing the recent progress on Pd-based electrocatalysts for electroreduction CO_2 to formic acid/formate.

Strategies to enhance ECO_2RR toward formic acid/formate of Pd-based electrocatalysts

As a precious metal catalyst, Pd-based catalysts have excellent catalytic activity and selectivity compared with other catalysts, which plays an irreplaceable role in many catalytic reactions, especially in ECO_2RR. Due to the formation of PdH_x in the reduction process, the variable active phases on the surface of Pd NPs determine the formation of *COOH or *OCHO intermediates[39,64], leading to the production of CO_2 to CO at high potentials and formic acid/formate at low potentials with high FEs[63]. In recent years, great efforts have been devoted to developing effective strategies on not only improving the formate activity and selectivity but also inhibiting CO poisoning and catalyst inactivation at high potentials. In the following sections, we will review nanoscale engineering strategies of Pd-based electrocatalysts for improving the catalytic performance toward formic acid/formate products, including size control, morphology and shape control, alloying, heteroatom doping, surface-strain engineering, and phase control. To aid readers in quickly capturing valuable and recapitulative information from related literature addressed in the following sections[31,34,40,65-74], we outlined the performances (potential, selectivity, current density, and stability) of various Pd-based related catalysts and their measurement conditions, including reactors and electrolyte solution, as shown in Table 1.

Size control

Size effect of metal NPs refers to the variation of catalytic performance with the particle size of the metal catalyst, which is intrinsically associated with the geometric and electronic properties[75-77]. On the one hand, in terms of geometric properties, it is well-established that decreasing size of NPs would improve the proportion of catalytically active surface or corner sites of NPs, thereby altering the ratio and distribution of catalytic centers[78,79]. On the other hand, from the perspective of electronic properties, the electron energy

Table 1. Performance comparison of representative Pd-based electrocatalysts for CO_2 reduction to formic acid/formate from recent literature

For formate product								
Strategies	**Electrocatalysts**	**Reactor type**	**Electrolytes**	**Potential at FE_{max} (V *vs.* RHE)**	**FE_{max} (%)**	**Current density/ mass activity**	**Stability**	**Ref.**
Size control	6.8 nm Pd NPs	H-type cell	0.5 M $NaHCO_3$	-0.1	98	452.3 ppm h^{-1} mg_{Pd}^{-1}	≈ 3,600 s	[65]
Morphology and shape control	s-mesoPdCu		0.1 M $KHCO_3$	-0.2	≈ 100	8.2 mA cm^{-2}	15,000 s	[66]
	Pd nanoparticles with high-index surfaces		0.5 M $KHCO_3$	-0.2	97	22 mA cm^{-2}	350 min	[67]
Alloying	PdSn/C NPs		0.5 M $KHCO_3$	-0.26	≈ 100	≈ 2 mA cm^{-2}	5 h	[31]
	PdAg_2		0.1 M $NaHCO_3$	≈ 0	≈ 100	3.6 mA cm^{-2}	10,000 s	[40]
	Pd_4Ag		0.1 M $KHCO_3$	≈ 0	90	6.0 mA cm^{-2}	15,000 s	[68]
	$Pd_{82}Cu_{18}$		0.1 M $KHCO_3$	-0.3	96	16.2 mA cm^{-2}	3 h	[69]
	np-PdCo		1 M $KHCO_3$	-0.2	≈ 100	≈ 20 mA cm^{-2}	4 h	[70]
Heteroatom doping	$PdH_{0.5}$/C		0.1 M $KHCO_3$	-0.4	93.1	1,787.7 μmol/h/mg_{Pd}	4 h	[71]
	Pd-B/C		0.1 M $KHCO_3$	-0.5	70	234 mM m^{-1}_{Pd}	2 h	[72]
Strain effect	M-AuPd(20)		0.5 M $KHCO_3$	-0.25	99	6.99 mA $cm^{-2}_{HCOO^-}$	3,600 s	[73]
Phase control	Pd_3Bi-IMA		0.1 M $KHCO_3$	-0.17	≈ 100	4.1 mA cm^{-2}	30,000 s	[74]
	Fully ordered PdBi NSs		0.5 M $KHCO_3$	-1.0	91.9	30.75 mA $_{HCOO^-}$	10 h	[34]

The pH of a solution of CO_2-saturated 0.1 M $KHCO_3$ or 0.1 M $NaHCO_3$ is 6.8, the pH of a solution of CO_2-saturated 0.5 M $KHCO_3$ or 0.5 M $NaHCO_3$ is 7.2, and the pH of a solution of CO_2-saturated 1 M $KHCO_3$ is 7.8.

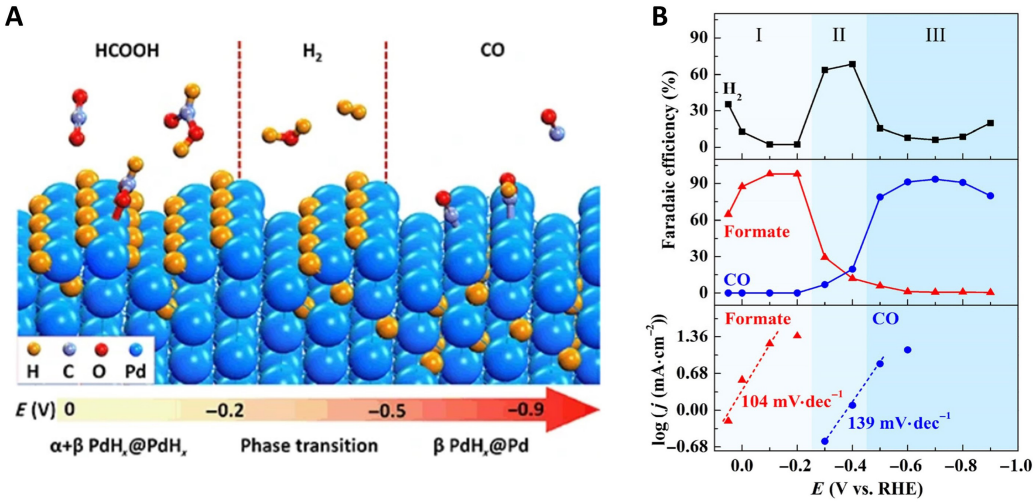

Figure 3. (A) Schematic diagram of switchable reaction pathways for CO_2 electroreduction caused by electrochemically-driven active-phase transformations of Pd nanoparticles[39]. Reprinted with permission. Copyright 2017, Springer[39]. (B) Faraday efficiency and the Tafel slope of formate, H_2 and CO at different potentials[39]. Reprinted with permission. Copyright 2017, Springer[39].

level of metal particles would be altered as the size changes, thus influencing the absorption energy of intermediates and determining the final products[80,81]. Consequently, to improve the product selectivity and study the size effect for CO_2RR catalytic activities based on different-sized Pd-based nanocatalysts, rational utilization size effect is of great significance.

In general, with the usage of chemical additives in the synthetic systems to regulate nucleation and growth dynamics, the size control can be achieved. Rahaman *et al.* prepared three types of Pd NPs within the size range of 3.8-10.7 nm by adjusting the molar ratio of polyvinylpyrrolidone (PVP) to Pd precursor and reaction temperature with $NaBH_4$ as reducing agent and PVP as capping agent [Figure 4A][65]. As shown in Figure 4B, Pd NPs with the medium-sized 6.5 nm deliver a formate FE of 98% at the potential of -0.1 V (*vs.* RHE); however, the selectivity toward formate further decreases with the particle size further increases, suggesting a high size-dependence of formate selectivity. The major reason for the selectivity differences is the formation rates of β-PdH phase on various sized Pd NPs and the competitive HER. Later, Gao *et al.* also studied the impact of NP size on product production activity and selectivity by systematically evaluating the ECO_2RR performance over Pd NPs with different sizes ranging from 2.4 to 10.3 nm[82]. These Pd NPs can efficiently reduce CO_2 to CO, and the FEs and catalytic current densities of CO were significantly improved with the decrease of particle size. The FEs for CO production over 2.4 and 3.7 nm Pd show the highest values among all the sizes, exceeding 80% across all the applied potential ranges [Figure 4C][82]. Based on three kinds of sites (terrace, edge, and corner) of Pd NPs, density functional theory (DFT) calculations reveal that the Gibbs free energies for the formation of COOH* on terrace (Pd (111)) are higher than those on stepped (Pd(221)) and corner (Pd55), indicating corner and edge sites are more active than terrace sites for the formation of COOH* intermediates [Figure 4D][82]. However, competitive HER has negligible differences on all these different active sites. Besides, LSV and CO stripping profiles over differently sized Pd NPs show a shift of peak potential of lower reduction potential of $Pd(OH)_2$ and weakened adsorption of CO with increasing particle size, which agrees well with the DFT calculations. Both the theoretical and experimental results suggest the nature of defected corner sites is beneficial to adsorb CO_2 and form the key reaction intermediates COOH* during CO_2 reduction. The optimal size having a high ratio of low-coordinated reaction sites significantly contributes to the high selectivity for CO production and current density.

Apart from NPs, Zhu *et al.* also studied the size effect on ultrathin hexagonal Pd nanosheets (NSs) ranging from 5.1 to 52.6 nm [Figure 4E and F], which were obtained via a one-pot chemical reduction method with CO gas and halide ions as adsorbent[83]. It is well known that ultrathin NSs with several atomic thicknesses process numerous low-coordinated edge sites[84,85]. Therefore, adjusting the edge length of the uniform NSs to control the ratio of reactive sites is a straightforward strategy to promote CO_2 conversion and investigate the size-dependent catalytic activity and selectivity. Among the different-sized NSs, CO FE of 5.1 nm Pd NSs displays the highest value, reaching up to 90% at a bias of -0.5 V, whereas 52.6 nm Pd just shows its maximum round 30% at -0.9 V, showing a high dependence on the edge length [Figure 4G][83]. In addition, the partial current densities also show a declined trend for CO production with the edge length increasing. Adjusting the size of Pd NPs also helps to improve the formate selectivity at low potentials. In the range of low overpotentials (-0.4 to -0.2 V), it was found that the formate FE over 5.1 nm Pd NSs was 76.4% at -0.2 V, outperforming the other counterparts. Such improvement in CO and formate FEs could be attributed to abundant low-coordinated sites. According to the generalized coordinated numbers of atoms, the authors classified the active sites at different positions of the NS and constructed a series of atomic models based on hexagonal NSs. DFT calculations demonstrate that edge sites and side facets whose generalized coordination number is 5-7 are in favor of CO production. With decreasing the edge length from 52.3 to 5.1 nm, the proportion of atomic with generalized coordination number of 5-7 gradually increased from 2.4% to 17.9%, showing a high dependence on the edge length of NSs. The computational calculations confirm that the formation of *COOH and CO desorption is much easier on specific active sites on the edge of NSs, well explaining the high CO selectivity of 5.1 nm Pd NSs with a high percentage of coordination number 5-7 sites. It should be noted that even though both studies focused on the size effect of Pd catalysts on CO selectivity, they are instructive for the study on formic acid/formate products. The applied biased potentials for both are in the range of high overpotential, which is the CO competing

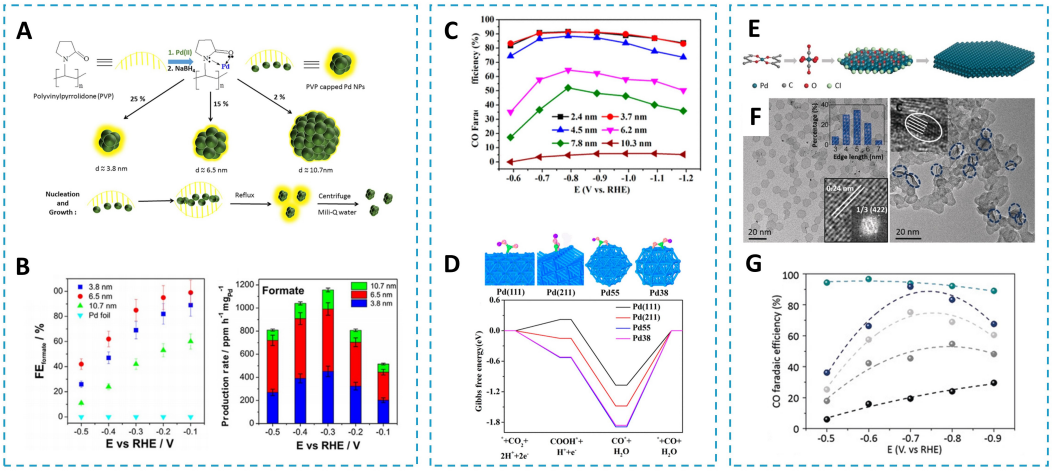

Figure 4. (A) Schematic diagram of the synthesis of Pd NPs with different sizes[65]. (B) FE and yield of formic acid at different potentials[65]. Reprinted with permission. Copyright 2017 WILEY[65]. (C) Free energy of COOH* adsorption and CO_2 reduction to CO on different crystal planes[82]. (D) Potential dependence of CO selectivity on different sized Pd NPs[82]. Reprinted with permission. Copyright 2015, American Chemical Society[82]. (E) Schematic diagram of the formation of hexagonal palladium NSs and (F) TEM images of palladium NSs with side lengths of 5.1 nm[83]. (G) CO Faraday efficiency of palladium NSs with different side lengths[83]. Reprinted with permission. Copyright 2018, WILEY[83].

dominated region. As such, the formation of *COOH intermediates is significantly facilitated within these potential ranges. Based on the fact that an electrochemically generated PdH_x surface has been an active site for formate generation, as mentioned previously, the applied potential dependence of formate FE is related to the PdH_x active phases. Even though experimental advances on size dependence of the selectivity towards formate, the real decisive factor for the formate selectivity enhancement over differently sized Pd NPs remains unclear. In this case, whether size-dependent electronic effects facilitate the formation of the PdH_x active phase needs further studies. Therefore, it is vital and significant to take DFT calculations to clarify the relationship between tunable ratios of active sites with different coordination numbers and Pd-H bond strength/catalytically active PdH_x phases to understand the size effect on CO_2RR.

Morphology and shape control

Except for the size-control strategy, morphology and shape control is a promising approach for improving the catalytic performance of Pd-based electrocatalysts[66,67,86]. Of central importance for catalyst design is maximizing the number of active sites on the surface. To this end, fabricating Pd nanocrystals (NCs) with complex structures provides the opportunity to create more reaction sites due to their highly tunable morphology and shape, resulting in the modification of the electronic structures. Based on the fact that heterogeneous catalysis occurs on the surface of catalysts, from the perspective of morphology, it is meaningful to create porous or hollow architecture to increase the roughness and enlarge surface area of the catalyst, which can create a larger active surface and expose more active sites in the case of constant geometric area[87]. Besides, it is well-known that different facets of NCs have unique coordination environments and intrinsic properties[87]. Therefore, exposing specific facets with more active sites is one of the intrinsic regulatory strategies to reduce the activation barriers, thereby boosting the selectivity and activity toward target products. In principle, in a typical synthesis of well-defined Pd-based NCs, the decisive key for the shape control is modulating thermodynamic and kinetic control of NC growth by tuning a set of experimental parameters, such as reducing agent, solvent, ligand, capping agent, surfactant, and extraneous ions. These capping agents, ions, solvents, and so on are selectively bound to a specific facet on NCs, determining the surface energies and growth rate for various facets[88]. As such, the anisotropic growth results in the formation of NCs with specific morphologies, shapes, or dimensions. The performance

of catalysts is usually closely related to their morphology because different morphologies and structures would influence the exposure of crystal facets and the proportion of corner, edge, and terrace atoms of NPs. Hence, morphology and shape control also provides a broad new notion for obtaining highly active and selective Pd-based catalysts for ECO_2RR.

Morphology and shape-controlled synthesis of metal NCs is crucial to creating effective catalysts and boosting the catalytic activity toward ECO_2RR[87]. Lv *et al.* adopted a facile soft template method to synthesize single-crystalline mesoporous Pd nanocubes (denoted as s-mesoPd)[66]. In the synthetic system, the quaternary ammonium salt was used as the surfactant template, and KCl worked as the facet-selective capping agent; both of them codetermine the precise control of the NC growth. The authors also explored diverse experimental parameters, including the carbon chain lengths of the surfactants, the extra Cl^- concentrations, and reaction times, and investigated their effects on structures and morphologies of the final products [Figure 5A][66]. Benefiting from large surface areas and rich mesoporous channels, s-mesoPdCu enabled a high formate selectivity over a broad potential window and achieved a FE approaching 100% at -0.2 V [Figure 5B]. Even the applied potential shifted as cathodic as -0.5 V, s-mesoPdCu still held its high selectivity and stability. The introduction of mesoporous greatly improves the charge transfer and dilutes CO coverage, which are responsible for enhanced CO tolerance, great stability and enlarged potential window [Figure 5C].

Surface engineering on specific shaped NCs has been proven to be a successful strategy to trigger high electrocatalytic activity for CO_2 electroreduction [Figure 5D][67]. It has been accepted that the surface atomic arrangement plays an important role in affecting the stabilization energies of active intermediates[89]. High-index facets possess a high density of low-coordinated sites, such as surface steps and kinks[90,91]. Such a feature offers abundant unsaturated dangling bonds on the surface, which are highly active for electrocatalytic reaction and affect the free energies required for the formation of intermediate and are usually very active for electrocatalytic reactions[90]. To promote the formation of *OCHO and inhibit *CO poisoning on the Pd surface during the CO_2-to-formic acid/formate conversion process, surface engineering on shaped NCs to create a rough surface with a mixture of high-index crystal facets may be preferable. By carrying out DFT calculation, Klinkova *et al.* elucidated that the binding energy of the HCOO* intermediates for formate product is more negative on high index facets, suggesting high-indexed facets with rough surface favored the HCOO* intermediates[67]. Besides, as the crystal index increases, the reaction energy barrier is obviously decreased, as shown by the free energy diagrams in Figure 5E[67]. According to the free energies of formation for HCOO* and CO* intermediates on different indexed facets [Figure 5F], high-indexed surface of Pd much more favors the formation of HCOO* rather than stabilizing CO* intermediate. However, the formation of CO* on the low-indexed surface shows a contrary trend. Besides, the findings from Bader partial atomic charges show that the charge density on the Pd atom bound to *CO significantly decreases as the surface index increases. Lower charge density suggests a weaker *CO binding strength on the high-index surface compared with low-index facets, implying less susceptibleness to CO intermediates. Projected density of states (PDOS) results further indicate that Pd (211) has stronger binding of HCOO* than that of Pd (111), further demonstrating more favorable adsorption for HCOO* on high-index surface[67]. All these results jointly support the argument that a high-indexed surface of Pd has a higher resistance to CO poisoning and simultaneously favors HCOOH production via HCOO*. The authors further prepared Pd nanocubes, rhombic dodecahedra, NPs with mixed low-index facets, and branched NPs enclosed by high-index facets to verify the catalytic behavior. Among these, branched NPs exhibit the highest current density of 22 mA cm^{-2} and formate FE of 97% at a low overpotential of -0.2 V. Computational simulations combined with electrochemical measurements verified that design and shape control of high-index surfaces is of great significance for improving intrinsic activity and selectivity toward CO_2 electroreduction.

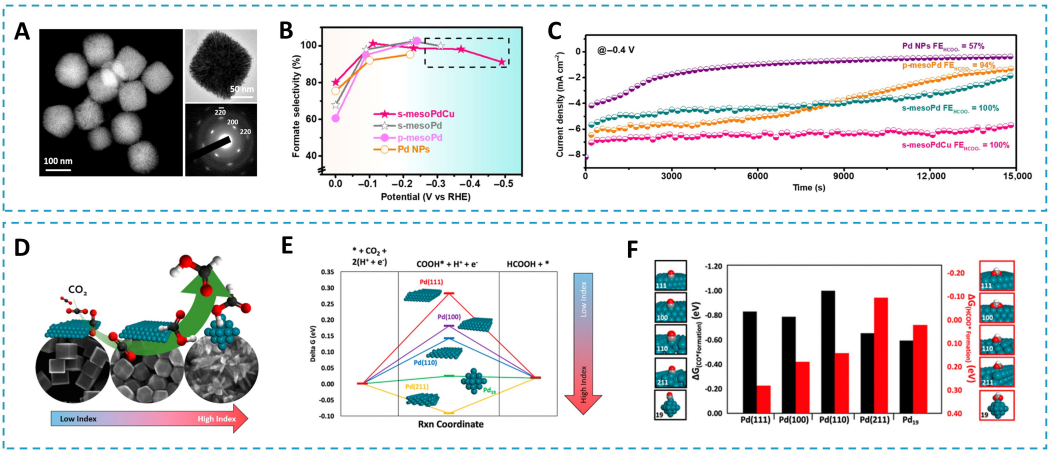

Figure 5. (A) STEM image of s-mesoPdCu nanocube[66]. Formic acid selectivities (B) and stability test at -0.4 V (C) for s-mesoPdCu, s-mesoPd, p-mesoPd and Pd NPs[66]. Reprinted with permission. Copyright 2018, Chinese Chemical Society[66]. (D) Schematic diagram of formic acid production over Pd nanocrystals enclosed by different crystal facets[67]. (E) Free energy of electrochemical reduction of CO_2 to formic acid on Pd(111) (red), Pd(100) (violet), Pd(110) (blue), Pd_{19} clusters (green) and Pd(211) (yellow)[67]. (F) HCOO* and *CO generate free energy on Pd nanocrystals with different crystal facets[67]. Reprinted with permission. Copyright 2016, American Chemical Society[67].

Alloying

Alloying with other metals has been considered as a successful strategy to develop highly active and stable Pd-based electrocatalysts[56,92,93]. Generally, the Pd-M alloy strategy not only reduces Pd content and the overall cost of electrocatalyst but also regulates the electronic structure of Pd based on the synthetic effect among the active components. Introducing a foreign metal into the host metal to form an alloy could trigger strong electron transfer, optimize electronic structures, and create more active sites, thus resulting in the altered adsorption energy for intermediates[94-96]. More importantly, in practical ECO_2RR, the modified electronic structure of Pd helps to improve the reaction kinetics and alter the surface atom configurations, thereby optimizing the bonding strength for reaction intermediates. These advantages can change the activity and product selectivity of electrocatalysts and thereby optimize catalytic performance.

To date, some progress has been made in improving the CO_2 reduction activity of Pd-based catalysts via a bimetallic alloy system. Compared with single-component Pd catalysts, the bimetallic palladium alloy showed better electrocatalytic activity and stability due to the alloy effect. Of note, the choice of secondary metal especially decides the variation in electronic structure of Pd and corresponding binding energy of intermediates. In recent years, researchers have devoted tremendous efforts to finely designing high-performance Pd-based electrocatalysts through alloying. A variety of bimetallic Pd alloys with other transition metals, such as tin (Sn)[31,97], silver (Ag)[33,40,68], gold (Au)[73,98,99], copper (Cu)[67,100,101], bismuth (Bi)[34,74], lead (Pb)[102], *etc.*, have been synthesized and displayed enhanced catalytic performance for CO_2-to-formic acid/formate conversion.

PdSn systems have been developed because Sn is a formate-selective metal and favorable to the formation of HCOO* intermediates[103]. Bai *et al.* have prepared Pd-Sn alloy NPs by varying the feeding ratio of the Pd and Sn salts[31]. In these series of Pd-Sn alloy NPs with different metal atomic ratios, the optimal sample PdSn/C with an equal molar ratio of Pd and Sn delivered an outstanding formic acid FE approaching 100% at the lowest overpotential of -0.26 V [Figure 6A and B]. A higher or lower Pd concentration in alloy leads

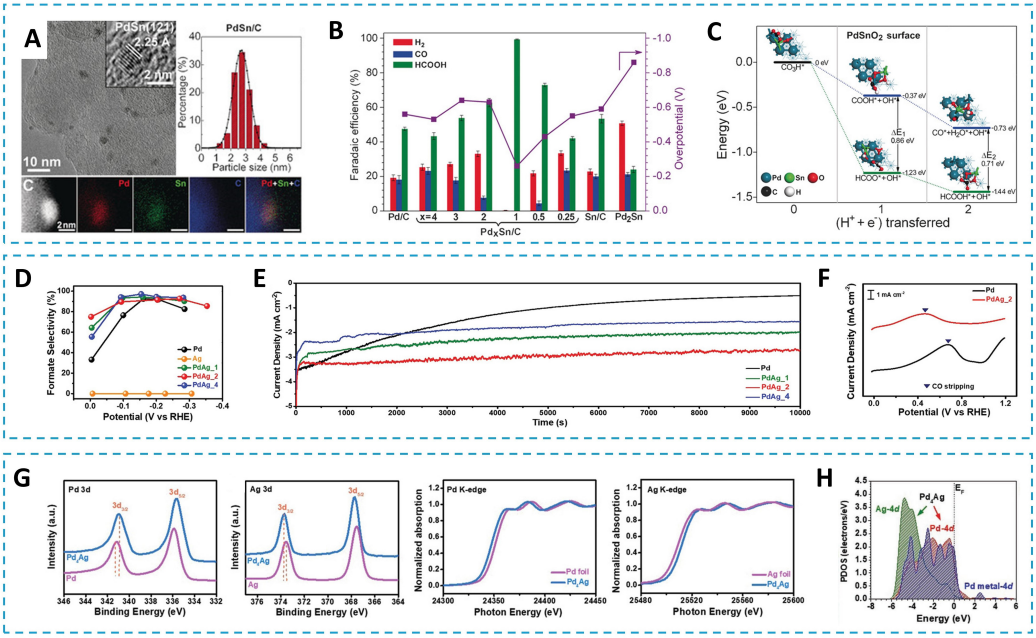

Figure 6. (A) Morphology characterization and size distribution of PdSn/C[31]. (B) Product FEs and overpotentials over Pd/C, Sn/C and alloy Pd_xSn/C under applied potentials[31]. (C) Energy calculation of CO_2 electroreduction to CO (top) and HCOO (bottom) on the surface of $PdSnO_2$[31]. Reprinted with permission. Copyright 2017, WILEY[31]. Formic acid selectivity (D), stability (E) and anodic oxidation peaks in LSV (F) of PdAg alloy with different chemical compositions[40]. Reprinted with permission. Copyright 2020, WILEY[40]. (G) XPS and XANES spectra of Pd_4Ag and pure Pd[68]. (H) PDOS of Pd_4Ag and pure Pd[68]. Reprinted with permission. Copyright 2020, WILEY[68].

to significant hydrogen evolution and thus lowers the formic acid selectivity and the catalytic activity. The relationship between the relative intensity ratio of Pd^0/Pd^{II} and the mole ratio of Pd/Sn exhibits a valley-shaped profile. On the surface of metal NPs, PdSn/C has the lowest Pd^0/Pd^{II} relative intensity ratio, implying a surface Pd-Sn-O layer derived from a certain amount of oxygen affinities on the PdSn alloy surface. DFT calculations revealed that it is favorable to form key reaction intermediate HCOO* and the production of HCOOH over the surface of $PdSnO_2$ whose Pd/Sn ratio is 1:1 [Figure 6C], which was matched well with the experimental results. The exclusive formation of formic acid can be attributed to optimized surface electronic structures induced with proper Pd-Sn-O layer. This study claimed that the PdSn alloy catalyst and its appropriate surface metal oxide configurations contributed to the favorable intermediates and CO_2-to-HCOOH pathway.

Ag, a well-known CO-generating metal, has an electron-rich state and intrinsic weak CO binding[104]. During ECO_2RR, at high overpotentials, CO is inevitably generated and strongly adsorbs on the Pd surface, causing Pd deactivation and consequently affecting the activity and product selectivity. Therefore, it is essential to introduce a secondary metal on the catalyst that can weaken the CO binding strength to maintain the formate production. As such, PdAg alloy would be an ideal case. Thus, to alleviate CO poisoning, Zhou *et al.* prepared mesoporous PdAg nanospheres with controlled atomic percentages by using cationic surfactant[40]. As seen in Figure 6D, among the samples, the best alloy candidate PdAg_2 composed of 62 wt% Pd and 38 wt% Ag exhibited impressive performance of superb formate FE close to 100% at zero overpotential and excellent stability. The improved CO tolerance of PdAg_2 nanospheres was reflected by long-time amperometric stability, CO stripping and anodic oxidation peaks in LSV [Figure 6E and F]. The electron redistribution of Pd and Ag atoms upon alloying well explained weakened CO surface

affinity and the resultant high selectivity and excellent stability toward CO_2-to-formate conversion. Thereafter, Han *et al.* further developed composition-controlled PdAg alloy nanowires with high aspect ratios and defected surfaces[68]. Benefiting from the electronic structure coupling with the one-dimensional structure with rough surface, the prepared Pd_4Ag nanowires achieved a high formate selectivity (90% FE at ≈ 0 V) and maintained the current density stable within 15,000 s at -0.43 V *vs.* RHE. Because of the higher electronegativity and lower work function of Ag relative to Pd, there is an electron transfer from Ag to Pd within the alloy, which was verified by X-ray photoelectron spectroscopy (XPS) and X-ray absorption near edge structure (XANES) spectra [Figure 6G]. In general, the d-band center is identified as a descriptor for electronic structure. With the cooperation of Ag, a down-shift of the d-band center occurs. The projected partial density of states (PDOS) of Pd_4Ag and pure Pd demonstrated the downshift of the d-band center with alloying with Ag, which was consistent with the experimental results [Figure 6H]. According to the DFT calculations, the production of the optimal d-band center mainly leads to the weakening of the binding of CO intermediates and Pd sites, thus promoting the formation of formate.

In addition, Pd-based electrocatalysts face a major challenge of a relatively narrow potential window for the selective production of formate. Cu is a metal that has a unique electronic property with moderate weakly *CO binding energy and smaller functions[105,106], which are lower than those of Pd. What is more, it is a high oxyphilic metal that is readily oxidized to form the surface metal oxide configuration, generating the new oxygen-containing sites. From this perspective, in our recent work, we alloyed Cu into the parent metal Pd to fabricate PdCu bimetallic dendritic NPs [Figure 7A][69]. In this case, the dendritic architectures, the ensemble effect between Pd and Cu atoms, and the surface oxygen-containing features synergistically contribute to the overall catalytic performance. Among all the Pd_xCu_y alloy catalysts, $Pd_{82}Cu_{18}$ displayed the highest formate FE of 96.0% at -0.3 V *vs.* RHE, with a broad potential window of 600 mV for the high selectivity (> 90%) [Figure 7B and C]. Here, the dendritic structure in our work principally provides a structural platform to improve all of the Pd-based catalysts. The formate FE and potential range over mono-component Pd catalysts are also superior to those of other reported Pd electrocatalysts. The alloy effect from the modified electronic structure and the optimal surface O-containing configuration seems to be the dominant reason for the enhancement in the formate selectivity and potential window.

The binding strength of *CO of Pd-based alloys is highly corrected with the selection of the secondary metal. To study this component-dependent catalytic behavior, Chatterjee *et al.* prepared free-standing, nanoporous Pd-X (np-PdX) alloys (X = Ni, Co, Ag, Cu) by electrochemical dealloying of $Pd_{15}X_{85}$ alloys[70]. After dealloying, the formed core-shell structure is composed of Pd skin and Pd-X alloy bulk [Figure 7D]. Here, the secondary metal components near the Pd-skin surface not only modify the electronic property but also modulate H-solubility. Ideal active Pd electrocatalysts have both weak H and CO bindings, simultaneously promoting CO_2 hydrogenations and CO destabilization. Accordingly, to seek optimal surface with the lowest H and CO binding strength, the authors performed DFT calculations based on six kinds of models, including CO* on clean surfaces, CO* on hydrogenated surfaces (*H and 2 *H), H* on clean surfaces, and H* on hydrogenated surfaces, and H* on a preadsorbed *CO surface. As shown in Figure 7E and F, in the low-energy surface configuration, the Pd-skin/Pd_3Co system exhibits the lowest binding energies of H* and *CO, which is coincident with the experimental trend of deactivation rate: np-PdAg > np-PdCu > Pd/C > np-PdNi > np-PdCo. Owing to the relatively weak *H and *CO binding, the Pd-skinned np-PdCo and np PdNi displayed a high formate selectivity and CO tolerance. According to both experimental and calculated results, the secondary metal component in np-PdX alloys influences the CO binding strength and H-sorption capacity in the near-surface, which jointly affect the observed deactivation behavior of catalyst under electrolysis.

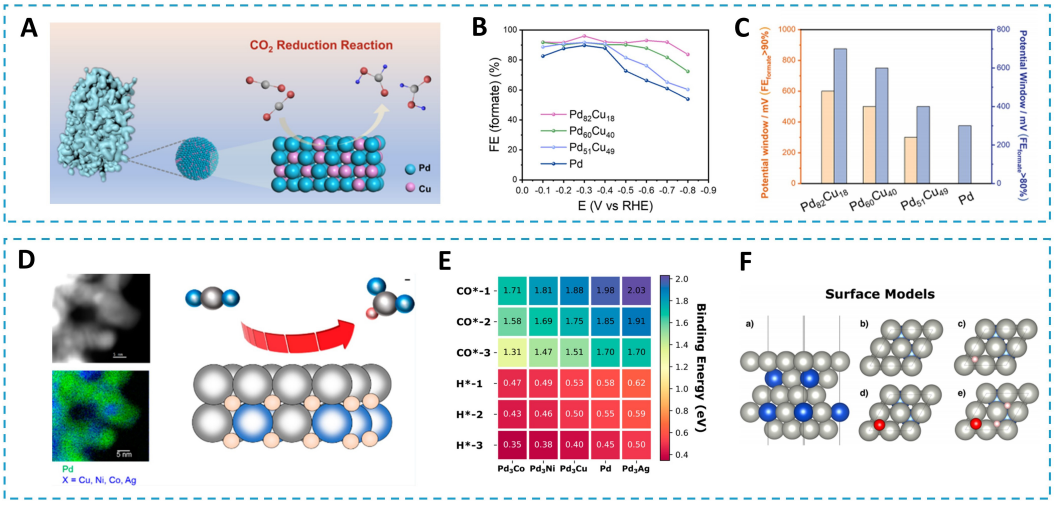

Figure 7. (A) Schematic diagram of formate production from a tunable composition PdCu bimetallic alloy catalyst based on dendrite structure[69]. (B) Potential dependence of formate FE on $Pd_{82}Cu_{18}$, $Pd_{60}Cu_{40}$, $Pd_{51}Cu_{49}$ and pure Pd[69]. (C) Comparison of potential windows of these four electrocatalysts with $FE_{formate}$ above 90% and 80%, respectively[69]. Reprinted with permission. Copyright 2022, American Chemical Society[69]. (D) Schematic diagram of formic acid production on nanoporous Pd alloy (np-PdX) formed by electrochemical dealloying of $Pd_{15}X_{85}$ alloy (X = Co, Ni, Cu and Ag)[70]. (E) Binding energies (eV) for CO combined with clean surfaces (CO*-1), CO with H*-containing surfaces (CO*-2), CO with 2H*-containing surfaces (CO*-3), H with clean surfaces (H*-1), H with H*-containing surfaces (H*-2), H with CO* containing surfaces (H*-3)[70]. (F) Side view of representative models of the Pd-skinned Pd_3X alloy used for calculations[70]. Reprinted with permission. Copyright 2019, American Chemical Society[70].

Heteroatom doping

Heteroatom doping, which refers to some nonmetal elements (such as H, B, N, and P) inserted into the lattice of host matrix and forms, has been extensively used to improve catalytic performance[71,107,108]. In the aforementioned section of Pd-based alloy, the secondary metal atoms generally substitute some parent metal atoms and occupy the location of Pd atoms. However, unlike the traditional bimetallic alloys, the foreign heteroatoms of an appropriate concentration occupy the interstices of the host metal lattice due to the small atomic radii of these light elements. In this case, heteroatom interstices could tune the lattice parameters and modify the electronic structure. Moreover, because of the high electronegativity of the light elements, the heteroatoms can induce the polarization of the surrounding atoms and alter the band centers of the active sites. So far, such an approach of interstitial heteroatom doping in Pd bulk has been adopted in various electrocatalysis applications, including oxygen reduction reaction, methanol oxidation reaction, HER, and ECO_2RR[71,109-111]. In particular, for electroreduction of CO_2 to formic acid/formate, designing heteroatom-doped Pd catalyst is a promising strategy to boost the electrocatalytic performance.

Hydrogen elements have the smallest atomic radii in the periodic table. Permeating hydrogen atoms into host Pd metal to form hydride could alter the electron density of Pd and thus change the binding strength of Pd with the reaction intermediates[112]. Accordingly, absorption of interstitial hydrogen atoms is identified to be a highly attractive method to trigger catalytic performance toward formate production in ECO_2RR. Previous studies have suggested that absorption of interstitial hydrogen atoms can weaken *CO adsorption, inhibit the CO poisoning, and facilitate the formation of formic acid/formate[38,39]. For example, Guo *et al.* synthesized a hydrogen-rich Pd hydride by adopting a one-step solvothermal synthesis route[71]. After inserting *in situ* hydrogen originating from the decomposition of organic solvent on Pd surface, a Pd hydride catalyst with a hydrogen content of around 0.5 was produced. The hydrogen content is lower than that of β-hydride (PdH_x, x~0.7), suggesting a mixture of the α- and β-phases in $PdH_{0.5}$/C. Because of the strong interactions between Pd and H, hydrogen atoms were directly inserted into the interstitial sites of the

Pd lattice, resulting in the lattice expansion. High-resolution transmission electron microscopy (HRTEM) images and X-ray diffraction (XRD) pattern results confirmed this phenomenon. Hence, the enlarged interplanar distance contributes to the downshift of the d-band center of Pd and the enhanced activity. Notably, $PdH_{0.5}$/C showed a formate FE of 93.1% at -0.4 V, far exceeding Pd/C catalyst. More importantly, CO poisoning study, CO stripping measurement, and stability tests certified that $PdH_{0.5}$/C had an outstanding CO tolerance, as shown in Figure 8A and B[71]. Using isotopic analysis, the authors experimentally confirmed that lattice hydrogen participated in the formate generation pathway and elucidated the crucial roles of lattice hydrogen and surface adsorbed H* species in the $HCOO^-$ formation pathway over $PdH_{0.5}$/C [Figure 8C][71]. In addition, the authors also proposed that the mutual diffusion behavior between the lattice hydrogen and the surface H* species derived from the proton species in electrolyte favored keeping a stable hydrogen-rich equilibrium composition during CO_2 electroreduction. This lattice hydrogen participated mechanism well explained the broadened electrochemical window for formate generation and suppressed formation toward CO.

In addition, Boron (B) insertion in the Pd lattice to form Pd-B alloy becomes an attractive way to promote ECO_2RR with a gratifying catalytic performance[113,114]. Boron, the lightest metalloid element in the IIIA group, has a relatively small electronegativity compared with other nonmetal elements. It has been demonstrated that B doping has a great beneficial effect on enhancing catalytic performance and hampering CO accumulation on Pd surface[109,115]. Taking advantage of the unique properties of B elements, Jiang *et al.* synthesized a boron-doped Pd catalyst (Pd-B/C) via a treatment method[72]. XRD patterns of Pd-B/C catalyst shifted negatively relative to those for Pd/C, indicative of a lattice expansion after doping B into Pd. XPS analysis revealed the electron transfer between Pd and B, which resulted in the downshift of the d-band center of Pd. With the synergy of optimized electronic structure by B, B-Pd interstitial NCs achieved a formate selectivity of 70% and a formate concentration of ca. 234 mM mg^{-1} Pd after 2 h of electrolysis at the potential of -0.5 V, outperforming Pd/C without B doping. The enhancement in formate selectivity and yield was ascribed to the B-doping effect, which was further confirmed by DFT calculations. It was found that, compared with Pd/C, B-doped Pd made the adsorption energy of HCOO* shift negatively and the Gibbs free energy for intermediates reduced [Figure 8D][72]. This suggests that the presence of B is more favorable for the HCOO* intermediates and formate pathway than the *COOH and CO pathway. On the basis of experimental observations and DFT calculations with and without B doping, the authors demonstrated the positive influence of the B doping on the formate pathway of CO_2RR [Figure 8E-G][72]. It is worth noting that Pd-B/C is a promising bifunctional catalyst for formic acid-CO_2 interconversion.

Strain effect

Surface strain widely exists in heterogeneous catalysis, and it is an effective method to modulate the electronic structure and thus influence its catalytic performance[116-118]. The strain effect, a long-range effect arising from lattice mismatch, reflects the lattice distortion and the change in the metal bond. According to the differences in lattice constants of metals in the shell/surface and in the bulk form, it can be classified into tensible and compressive strain. A tensible shell with an enlarged interatomic distance is produced when introducing a foreign metal with a larger lattice constant than that of Pd[119]. On the contrary, introducing a metal with a smaller lattice constant would generate a compressive-strained shell with a shortened interatomic distance[120]. The interatomic distance displays a direct impact on the d-band center of host metal. It is well established that the d-band center is widely used to describe the change of electronic structure of catalyst[121]. The above-mentioned subtle changes in atomic distance of the metals result in the surface atoms being either enlarged or compressed, leading to a shift in the d-band center and, thus, a variation in binding strength toward intermediates. The former causes an upshift of the d-band center, strengthening the binding strength, whereas the latter induces a downshift of the d-band center, weakening the interaction. Encouraged by the strain effect, constructing effective Pd nanocatalysts by altering the

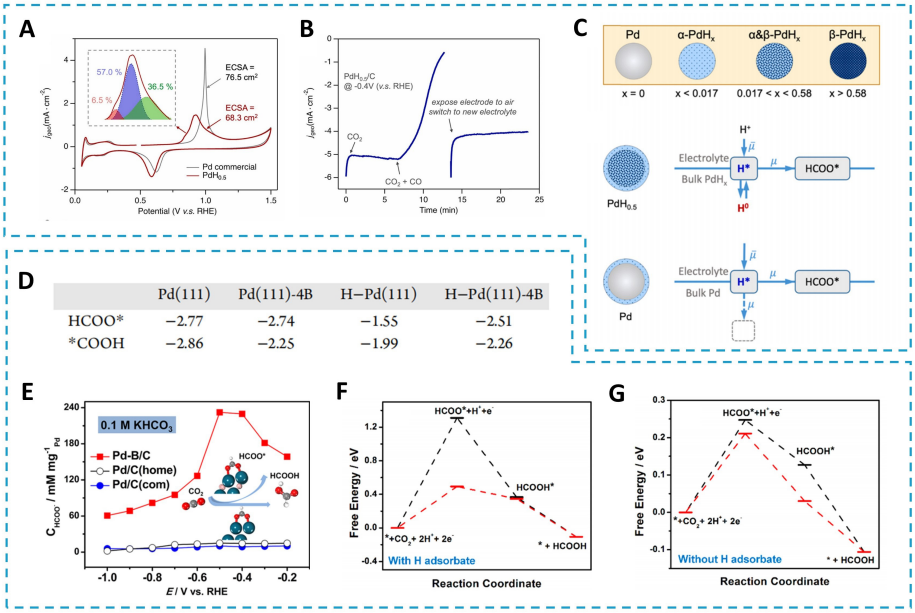

Figure 8. (A) CO stripping measurement of $PdH_{0.5}$/C and Pd/C[71]. (B) CO tolerance tests for $PdH_{0.5}$/C at -0.4 V *vs.* RHE in CO_2-saturated 0.1 M $KHCO_3$ electrolyte[71]. (C) Reaction mechanism for $HCOO^-$ generation on $PdH_{0.5}$/C catalysts[71]. Reprinted with permission. Copyright 2022, Elsevier[71]. (D) Calculated surface adsorption energies (eV) of HCOO* and *COOH on Pd(111) and Pd(111)-4B with and without H adsorption[72]. (E) Potential dependence of mass normalized formate concentration on Pd-B/C catalysts[72]. Gibbs free energy diagrams for the intermediates in formate pathway on Pd-B/C (red) and Pd/C (black) with (F) and without (G) hydrogen adsorption[72]. Reprinted with permission. Copyright 2018, American Chemical Society[72].

atomic spacing of surface atoms to tune the binding strength toward intermediates is welcome for promoting ECO_2RR[122].

Recently, Bok *et al.* used tensile strain effect from the confined AuPd NPs to boost CO electroreduction to formate[73]. They synthesized atomically dispersed Au on tensile-strained Pd NPs anchored in the confined space of metal-organic frameworks (MOFs) via a confined reduction method [Figure 9A and B]. By analyzing the lattice spacing from aberration-corrected transmission electron microscope (Cs-TEM) image, the authors confirmed the existence of tensile strain and lattice distortions in M-AuPd(x), where x represents the ratio of Au. The tensile strain induced in the Au atom-doped Pd NPs originates from the metal-MOF interaction, as shown in Figure 9C and D. With the precise adjustment of strain effect, a remarkable enhanced catalytic activity was found over M-AuPd(20), reaching an outstanding formate FE over 99% at -0.25 V *vs.* RHE [Figure 9E]. Besides, the current density and mass activity of M-AuPd(20) was increased by 26 and 31 times compared with Pd/C. DFT calculations enclosed the origin for the enhanced electrocatalytic performance for formate production. The synergy between tensile strain effect in Pd surface and electronic effect from atomically dispersed Au incorporation contributes to the improved electrocatalytic performance in terms of activity, formate selectivity and stability. In the electrocatalysis process, these two effects generally function together synchronously to break the scaling relationship of COOH* *vs.* CO* intermediates and, thus, ultimately determine the catalytic behavior. On the one hand, the generating tensile strain in Pd surface stabilizes the intermediate species COOH* and HCOO* and facilitates CO_2 activation. On the other hand, dispersed Au atoms destabilize CO* to suppress CO poisoning without affecting other intermediates. This work highlights the important role of strain effect in promoting electrocatalysis for formate production from CO_2.

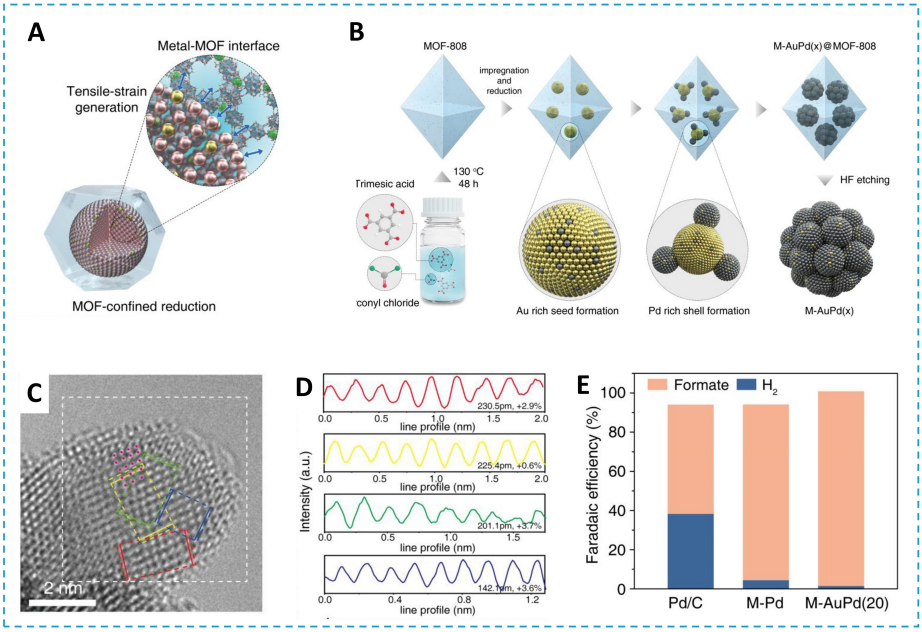

Figure 9. (A) Tensile strain effects generated on AuPd alloy nanoparticle through MOF-confined reduction[73]. (B) Schematic diagram of the preparation of M-AuPd(x) catalyst[73]. (C) Representative Cs-TEM image of M- AuPd(20)[73]. (D) Intensity profile measured from the area indicated by the colored rectangular box from (C)[73]. (E) Comparison of formate Faraday efficiency of Pd/C, M-Pd and M-AuPd(20)[73]. Reprinted with permission. Copyright 2021, American Chemical Society[73].

Phase control

For Pd-based electrocatalysts, phase control has recently emerged as a promising tactic to optimize their catalytic performance. Solid-solution alloy with disordered atomic arrangement is the most common type of metal alloy[123,124]. Compared to disordered solid solution alloy, ordered intermetallic compound has a specific atom stoichiometric ratio and long-range atomic ordering, leading to strong interatomic interaction[125]. Even though they have the same stoichiometry as random alloys, the physico-chemical properties of intermetallic compounds are significantly distinct. Profiting from the features, intermetallic compounds exhibit unique properties and great potential in various applications[91,126,127]. Consequently, it is particularly appealing for ECO_2RR to construct robust Pd-based multimetallic NCs through phase engineering. More importantly, in-depth study of phase-dependent activity and selectivity of catalyst is of great significance for electrocatalyst design.

Jia *et al.* synthesized Pd_3Bi intermetallic alloys (IMAs) with a fixed stoichiometry of 3/1 and uniform sizes by adopting a facile solvothermal method[74]. It is well accepted that a solvothermal method provides a versatile approach to synthesizing intermetallic compounds. The ordered NCs can be transformed into a random solid solution alloy (Pd_3Bi-SSA) through thermal annealing at 500 °C, as illustrated in Figure 10A. By manipulating the atomic ordering, the phase-performance relationship was investigated. Impressively, electrochemical measurement for ECO_2RR of Pd_3Bi IMAs holds an excellent formate selectivity of approximately 100% and high stability even at a bias of < -0.35 V, exceeding vast majority of Pd-based materials reported in the literature[128,129]. By contrast, Pd_3Bi-SSA is greatly inferior to Pd_3Bi IMAs in terms of formate selectivity and CO poisoning resistance. To reveal the influence of atomic ordering on the catalytic performance toward formate generation, DFT simulations were conducted. According to the PDOS analysis, adsorption energies of key adsorbates, and energetic trend, the favorable formation and stabilized adsorption of *OCHO on Pd_3Bi IMAs was validated. Experimental observations, coupled with theoretical calculation, corroborate that ordered phase endows PdBi alloy with enhanced CO_2RR performance. This

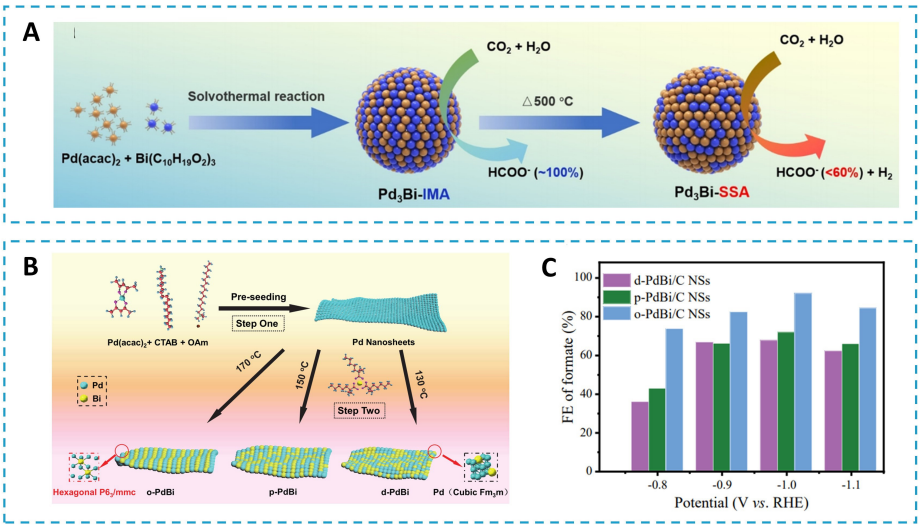

Figure 10. (A) Schematic diagram of the synthesis of Pd_3Bi-IMA and Pd_3Bi-SSA[74]. Reprinted with permission. Copyright 2021, WILEY[74]. (B) Schematic diagram of the synthesis of fully ordered (o-), partially ordered (p-) and disordered (d-) PdBi NS[34]. (C) Formate selectivity at different applied potentials[34]. Reprinted with permission Copyright 2022, Elsevier[34].

work emphasizes the important role of phase engineering in influencing catalytic behavior and electrochemical CO_2-to-formate activity.

Likewise, taking advantage of phase engineering, Xie *et al.* reported intermetallic PdBi NSs with ordered hexagonal phase as electrocatalysts for ECO_2RR[34]. In the synthetic process of PdBi NSs, the ordering degree of Pd and Bi atoms in crystallographic structures can be finely tuned by controlling the synthesizing temperature. To accurately evaluate the structure-ECO_2RR performance relationship of PdBi NSs, they prepared three types of Pd-based NSs for comparison, as shown in Figure 10B. PdBi alloy with completed ordered phase was found to be exceptionally selective and active for producing formate. Compared to disordered PdBi NSs, partially ordered PdBi NSs, and pure Pd NSs, intermetallic PdBi NSs delivered a high formate FE of 91.9% at -1.0 V and a wide potential window [Figure 10C]. DFT calculations indicated that a free energy barrier for *OCHO adsorption on the Bi surface in fully ordered PdBi NSs is 0.13 eV, lower than that in disordered PdBi NS, which is mainly responsible for the enhanced catalytic performance.

CONCLUSION AND PERSPECTIVES

Electrochemically converting CO_2 into formic acid/formate using renewable electricity is a promising technology to effectively alleviate global warming and solve the energy issues because of its economic feasibility, environmental benignancy and product values. Among various metal materials, Pd stands out due to its unique property of intrinsically preferable selectivity toward formic acid/formate approaching minimal overpotential. In this review, we summarize the most recent progress of innovative design strategies of fabricating effective Pd-based electrocatalysts for ECO_2RR conversion into formic acid/formate. Diverse innovative design strategies, including size control, shaping nanomaterials, alloying, heteroatom doping, surface-strain engineering, and phase control, are comprehensively discussed. In these cases, active site concentration, intrinsic electronic structures of the catalytic materials and their interaction with the reaction intermediates were modified, leading to significant improvements in performance. Moreover, experimentally and theoretically understanding the structure-performance relationship and the promoting principle provide a deep insight into the reaction mechanism over Pd-based catalysts. Although great efforts have been made, most Pd-based catalysts face great challenges because of their high cost and in-situ

reconstruction issues during the CO_2RR process, and resultant decreased current density, reduced activity, and poor stability. These limitations critically restrict the large-scale application of Pd-based catalysts in ECO_2RR. By now, the electrocatalytic efficiency and stability are mostly in the proof-of-concept stage, far from industrialization. Many prosperous opportunities should be grasped, and new challenges should be addressed in some specific aspects, such as high reaction currents and energy efficiencies, for the future development.

From the viewpoint of practical operation, the cost of electrocatalysts should be taken into consideration. It is well established that, for heterogeneous electrocatalysis, an electrocatalysis process occurs on catalyst surface and the surface participates in activating chemical bonds. The atomic arrangements and chemical compositions in the catalyst surface greatly influence overall catalytic performance. Thus, developing advanced synthetic strategy to obtain Pd NCs with precisely controlled surface and rich CO_2RR-preferential sites is of great significance to improve the intrinsic activity and the atomic utilization efficiency of Pd. Designing clusters or single-atom structures will be an alternative way to increase atomic utilization. The d-valence electrons of transition metal atoms in single-atom structures are close to the Fermi level, enabling rapid electron transfer and facilitating the adsorption of CO_2 intermediates, thereby lowering the energy barriers of the reaction intermediates[130]. Besides, construction of compositional segregated surface by inducing atomic migration from bulk to surface under different atmospheres/temperatures conditions may be an alternative way to modify the surface electronic structure to improve the intrinsic activity.

Considering the industrial scale of CO_2 conversion, the current density and energy efficiency, which determine the overall cost, are a great challenge. Currently, the majority of research on Pd-based catalysts is conducted in an H-type electrolysis cell with $KHCO_3$ as the electrolyte; however, the current densities and reaction rates are far from enough for the industrial requirements. In this conventional H-type cell system, ECO_2RR suffers from drawbacks such as low CO_2 solubility and mass transfer limitations, so current density cannot meet the requirements for industrial production (> 200 mA cm^{-2}). In this case, to overcome CO_2 solubility and the mass transport issues, gas diffusion electrodes (GDE) are employed to reduce the CO_2 diffusion path, leading to order-of-magnitude increase in current densities. Although considerable progress in current density has been achieved using GDE configuration, there are some technological challenges in GDE, such as high ohmic resistance and low energy efficiency[131-133]. To address these key challenges, developing and optimizing advanced electrochemical devices for practical operation, especially membrane-electrode assembly (MEA) electrolyzers and their assembled stack, will become a new research hotspot. Efforts are also needed to further optimize the reactor constructions and the membranes in the electrochemical devices to meet industrial requirements and ensure market compatibility.

Apart from the catalysts and electrolyzers, the critical importance of mechanism study needs to be highlighted. Despite some success in DFT calculations and characterization techniques (such as synchrotron X-ray absorption spectroscopy (XAS) and *in situ* Raman) to study the reaction mechanism and reaction path, the majority of the studies have focused on the adsorption property and reaction pathway. Identifying and visualizing real active sites for multicomponent alloy and tracking dynamic evolution of nanostructures during electrocatalysis is still lacking; thus, some combined *in situ* characterization techniques, such as transmission electron microscopy (TEM) and XAS, are highly welcome[134,135]. Monitoring the real active sites, active phase, catalyst structural evolution, and chemical states of catalyst using *operando* characterization techniques for electrocatalysis during the reaction process helps to deepen understanding and illustrate the catalytic mechanism of Pd-based catalysts.

DECLARATIONS

Authors' contributions

Conceptualization and funding acquisition, writing-review & editing, and supervision: Liu X
The investigation, visualization, and writing-original draft: Sun S, Mao Y, Liu F, Zhang S, Sun Y
Helped to guide the review, including language checking and polishing: Gao Q

Availability of data and materials

Not applicable.

Financial support and sponsorship

This work was supported by the National Natural Science Foundation of China (22379066, 21603209, 52173173, and 21975124), the Natural Science Foundation of Jiangsu Province (BK20220051), Jiangsu Province Carbon Peak and Neutrality Innovation Program (Industry tackling on prospect and key technology) (BE2022031-4, BE2022002-3), and the Postgraduate Research & Practice Innovation Program of Jiangsu Province (KYCX23_1406).

Conflicts of interest

All authors declared that there are no conflicts of interest.

Ethical approval and consent to participate

Not applicable.

Consent for publication

Not applicable.

REFERENCES

1. Luna P, Hahn C, Higgins D, Jaffer SA, Jaramillo TF, Sargent EH. What would it take for renewably powered electrosynthesis to displace petrochemical processes? *Science* 2019;364:eaav3506. DOI PubMed
2. Bushuyev OS, De Luna P, Dinh CT, et al. What should we make with CO_2 and how can we make it? *Joule* 2018;2:825-32. DOI
3. Sa YJ, Lee CW, Lee SY, Na J, Lee U, Hwang YJ. Catalyst-electrolyte interface chemistry for electrochemical CO_2 reduction. *Chem Soc Rev* 2020;49:6632-65. DOI
4. Lei Y, Wang Z, Bao A, et al. Recent advances on electrocatalytic CO_2 reduction to resources: target products, reaction pathways and typical catalysts. *Chem Eng J* 2023;453:139663. DOI
5. Shakun JD, Clark PU, He F, et al. Global warming preceded by increasing carbon dioxide concentrations during the last deglaciation. *Nature* 2012;484:49-54. DOI
6. Khezri B, Fisher AC, Pumera M. CO_2 reduction: the quest for electrocatalytic materials. *J Mater Chem A* 2017;5:8230-46. DOI
7. Tanvir RU, Zhang J, Canter T, Chen D, Lu J, Hu Z. Harnessing solar energy using phototrophic microorganisms: a sustainable pathway to bioenergy, biomaterials, and environmental solutions. *Renew Sustain Energy Rev* 2021;146:1-111181. DOI PubMed PMC
8. Zhu DD, Liu JL, Qiao SZ. Recent Advances in inorganic heterogeneous electrocatalysts for reduction of carbon dioxide. *Adv Mater* 2016;28:3423-52. DOI PubMed
9. Zhu S, Delmo EP, Li T, et al. Recent advances in catalyst structure and composition engineering strategies for regulating CO_2 electrochemical reduction. *Adv Mater* 2021;33:e2005484. DOI
10. Wang Y, Miao Y, Ge B, et al. Additives enhancing supported amines performance in CO_2 capture from air. *SusMat* 2023;3:416-30. DOI
11. Gu Z, Shen H, Shang L, Lv X, Qian L, Zheng G. Nanostructured copper-based electrocatalysts for CO_2 reduction. *Small Methods* 2018;2:1800121. DOI
12. Liu C, Gallagher JJ, Sakimoto KK, et al. Nanowire-bacteria hybrids for unassisted solar carbon dioxide fixation to value-added chemicals. *Nano Lett* 2015;15:3634-9. DOI PubMed PMC
13. Lu Q, Rosen J, Zhou Y, et al. A selective and efficient electrocatalyst for carbon dioxide reduction. *Nat Commun* 2014;5:3242. DOI

14. Qiao J, Liu Y, Hong F, Zhang J. A review of catalysts for the electroreduction of carbon dioxide to produce low-carbon fuels. *Chem Soc Rev* 2014;43:631-75. DOI
15. Li Z, Qi X, Wang J, et al. Stabilizing highly active atomically dispersed NiN_4Cl sites by Cl-doping for CO_2 electroreduction. *SusMat* 2023;3:498-509. DOI
16. Liu S, Fan Y, Wang Y, et al. Surface-oxygen-rich Bi@C nanoparticles for high-efficiency electroreduction of CO_2 to formate. *Nano Lett* 2022;22:9107-14. DOI
17. Şahin NE, Comminges C, Arrii S, Napporn TW, Kokoh KB. CO_2-to-HCOOH electrochemical conversion on nanostructured Cu_xPd_{100-x}/carbon catalysts. *ChemElectroChem* 2021;8:1362-8. DOI
18. Sun Y, Liu F, Wang X, et al. Highly selective CO_2 electroreduction to CO by the synergy between Ni-N-C and encapsulated Ni nanoparticles. *Dalton Trans* 2023;52:928-35. DOI
19. Frese KW, Leach S. Electrochemical reduction of carbon dioxide to methane, methanol, and CO on Ru electrodes. *J Electrochem Soc* 1985;132:259-60. DOI
20. Wang P, Yang H, Tang C, et al. Boosting electrocatalytic CO_2-to-ethanol production via asymmetric C-C coupling. *Nat Commun* 2022;13:3754. DOI PubMed PMC
21. Zhang H, Gao J, Raciti D, Hall AS. Promoting Cu-catalysed CO_2 electroreduction to multicarbon products by tuning the activity of H_2O. *Nat Catal* 2023;6:807-17. DOI
22. De R, Gonglach S, Paul S, et al. Electrocatalytic reduction of CO_2 to acetic acid by a molecular manganese corrole complex. *Angew Chem Int Ed* 2020;132:10614-21. DOI
23. Liu X, Zhang K, Sun Y, et al. Upgrading CO_2 into acetate on Bi_2O_3@carbon felt integrated electrode via coupling electrocatalysis with microbial synthesis. *SusMat* 2023;3:235-47. DOI
24. Zhang H, Qiao Y, Wang Y, Zheng Y, Huang H. *In situ* oxidative etching-enabled synthesis of hollow Cu_2O nanocrystals for efficient CO_2 RR into C_{2+} products. *Sustain Energy Fuels* 2022;6:4860-5. DOI
25. Han N, Ding P, He L, Li Y, Li Y. Promises of main group metal-based nanostructured materials for electrochemical CO_2 reduction to formate. *Adv Energy Mater* 2020;10:1902338. DOI
26. Jouny M, Luc W, Jiao F. General techno-economic analysis of CO_2 electrolysis systems. *Ind Eng Chem Res* 2018;57:2165-77. DOI
27. Calle-Vallejo F, Koper MT. Theoretical considerations on the electroreduction of CO to C_2 species on Cu(100) electrodes. *Angew Chem Int Ed* 2013;52:7282-5. DOI PubMed
28. Schreier M, Luo J, Gao P, Moehl T, Mayer MT, Grätzel M. Covalent immobilization of a molecular catalyst on Cu_2O photocathodes for CO_2 reduction. *J Am Chem Soc* 2016;138:1938-46. DOI PubMed
29. Hori Y, Takahashi I, Koga O, Hoshi N. Selective formation of C_2 compounds from electrochemical reduction of CO_2 at a series of copper single crystal electrodes. *J Phys Chem B* 2002;106:15-7. DOI
30. Wulan B, Cao X, Tan D, et al. To stabilize oxygen on In/In_2O_3 heterostructure via joule heating for efficient electrocatalytic CO_2 reduction. *Adv Funct Mater* 2022;33:2209114. DOI
31. Bai X, Chen W, Zhao C, et al. Exclusive formation of formic acid from CO_2 electroreduction by a tunable Pd-Sn alloy. *Angew Chem Int Ed* 2017;56:12219-23. DOI
32. Li P, Yang F, Li J, et al. Nanoscale engineering of P-block metal-based catalysts toward industrial-scale electrochemical reduction of CO_2. *Adv Energy Mater* 2023;13:2301597. DOI
33. Chen Z, Wang X, Wang L, Wu YA. Ag@Pd bimetallic structures for enhanced electrocatalytic CO_2 conversion to CO: an interplay between the strain effect and ligand effect. *Nanoscale* 2022;14:11187-96. DOI
34. Xie L, Liu X, Huang F, et al. Regulating Pd-catalysis for electrocatalytic CO_2 reduction to formate via intermetallic PdBi nanosheets. *Chin J Catal* 2022;43:1680-6. DOI
35. Goswami C, Borah BJ, Das R, et al. CeO_2 promotes electrocatalytic formic acid oxidation of Pd-based alloys. *J Alloys Compd* 2023;948:169665. DOI
36. Liu M, Chen X, Wang Z, et al. Size-controlled palladium nanoparticles encapsulated in silicalite-1 for methane catalytic combustion. *ACS Appl Nano Mater* 2023;6:3637-46. DOI
37. Ma K, Liao W, Shi W, et al. Ceria-supported Pd catalysts with different size regimes ranging from single atoms to nanoparticles for the oxidation of CO. *J Catal* 2022;407:104-14. DOI
38. Liu G, Poths P, Zhang X, et al. CO_2 hydrogenation to formate and formic acid by bimetallic palladium-copper hydride clusters. *J Am Chem Soc* 2020;142:7930-6. DOI
39. Gao D, Zhou H, Cai F, et al. Switchable CO_2 electroreduction via engineering active phases of Pd nanoparticles. *Nano Res* 2017;10:2181-91. DOI
40. Zhou Y, Zhou R, Zhu X, et al. Mesoporous PdAg nanospheres for stable electrochemical CO_2 reduction to formate. *Adv Mater* 2020;32:e2000992. DOI
41. Zhou R, Fan X, Ke X, et al. Two-dimensional palladium-copper alloy nanodendrites for highly stable and selective electrochemical formate production. *Nano Lett* 2021;21:4092-8. DOI
42. Chang X, Wang T, Gong J. CO_2 photo-reduction: insights into CO_2 activation and reaction on surfaces of photocatalysts. *Energy Environ Sci* 2016;9:2177-96. DOI
43. Jiao L, Yang W, Wan G, et al. Single-atom electrocatalysts from multivariate metal-organic frameworks for highly selective reduction of CO_2 at low pressures. *Angew Chem Int Ed* 2020;59:20589-95. DOI

44. Appel AM, Bercaw JE, Bocarsly AB, et al. Frontiers, opportunities, and challenges in biochemical and chemical catalysis of CO_2 fixation. *Chem Rev* 2013;113:6621-58. DOI PubMed PMC
45. Torrente-murciano L, Mattia D, Jones M, Plucinski P. Formation of hydrocarbons via CO_2 hydrogenation - a thermodynamic study. *J CO2 Util* 2014;6:34-9. DOI
46. Wu J, Sharma PP, Harris BH, Zhou X. Electrochemical reduction of carbon dioxide: IV dependence of the Faradaic efficiency and current density on the microstructure and thickness of tin electrode. *J Power Sources* 2014;258:189-94. DOI
47. Tekalgne MA, Do H, Hasani A, et al. Two-dimensional materials and metal-organic frameworks for the CO_2 reduction reaction. *Mater Today Adv* 2020;5:100038. DOI
48. Zhang W, Hu Y, Ma L, et al. Progress and perspective of electrocatalytic CO_2 reduction for renewable carbonaceous fuels and chemicals. *Adv Sci* 2018;5:1700275. DOI PubMed PMC
49. Kuang Y, Rabiee H, Ge L, et al. High-concentration electrosynthesis of formic acid/formate from CO_2: reactor and electrode design strategies. *Energy Environ Mate* 2023;6:e12596. DOI
50. Durand WJ, Peterson AA, Studt F, Abild-pedersen F, Nørskov JK. Structure effects on the energetics of the electrochemical reduction of CO_2 by copper surfaces. *Surf Sci* 2011;605:1354-9. DOI
51. Kyriacou G, Anagnostopoulos A. Electrochemical reduction of CO_2 at Cu + Au electrodes. *J Electroanal Chem* 1992;328:233-43. DOI
52. Koga O, Hori Y. Reduction of adsorbed Co on a Ni electrode in connection with the electrochemical reduction of CO_2. *Electrochim Acta* 1993;38:1391-4. DOI
53. Kostecki R, Augustynski J. Electrochemical reduction of CO_2 at an activated silver electrode. *Ber Bunsenges Phys Chem* 1994;98:1510-5. DOI
54. Murata A, Hori Y. Product selectivity affected by cationic species in electrochemical reduction of CO_2 and CO at a Cu Electrode. *Bull Chem Soc Jpn* 1991;64:123-7. DOI
55. Saha P, Amanullah S, Dey A. Selectivity in electrochemical CO_2 reduction. *ACC Chem Res* 2022;55:134-44. DOI PubMed
56. Ulissi ZW, Tang MT, Xiao J, et al. Machine-learning methods enable exhaustive searches for active bimetallic facets and reveal active site motifs for CO_2 reduction. *ACS Catal* 2017;7:6600-8. DOI
57. Nie X, Luo W, Janik MJ, Asthagiri A. Reaction mechanisms of CO_2 electrochemical reduction on Cu(111) determined with density functional theory. *J Catal* 2014;312:108-22. DOI
58. Wu J, Huang Y, Ye W, Li Y. CO_2 reduction: from the electrochemical to photochemical approach. *Adv Sci* 2017;4:1700194. DOI PubMed PMC
59. Rosen J, Hutchings GS, Lu Q, et al. Mechanistic insights into the electrochemical reduction of CO_2 to CO on nanostructured Ag surfaces. *ACS Catal* 2015;5:4293-9. DOI
60. Montoya JH, Shi C, Chan K, Nørskov JK. Theoretical insights into a CO dimerization mechanism in CO_2 electroreduction. *J Phys Chem Lett* 2015;6:2032-7. DOI PubMed
61. Hori Y, Kikuchi K, Suzuki S. Production of CO and CH4 in electrochemical reduction of CO2 at metal electrodes in aqueous hydrogencarbonate solution. *Chem Lett* 1985;14:1695-8. DOI
62. Kuhl KP, Cave ER, Abram DN, Jaramillo TF. New insights into the electrochemical reduction of carbon dioxide on metallic copper surfaces. *Energy Environ Sci* 2012;5:7050. DOI
63. Gao D, Zhou H, Cai F, Wang J, Wang G, Bao X. Pd-containing nanostructures for electrochemical CO_2 reduction reaction. *ACS Catal* 2018;8:1510-9. DOI
64. Diercks JS, Herranz J, Georgi M, et al. Interplay between surface-adsorbed CO and bulk Pd hydride under CO_2 -electroreduction conditions. *ACS Catal* 2022;12:10727-41. DOI
65. Rahaman M, Dutta A, Broekmann P. Size-dependent activity of palladium nanoparticles: efficient conversion of CO_2 into formate at low overpotentials. *ChemSusChem* 2017;10:1733-41. DOI PubMed
66. Lv H, Lv F, Qin H, et al. Single-crystalline mesoporous palladium and palladium-copper nanocubes for highly efficient electrochemical CO_2 reduction. *CCS Chem* 2022;4:1376-85. DOI
67. Klinkova A, De Luna P, Dinh C, et al. Rational design of efficient palladium catalysts for electroreduction of carbon dioxide to formate. *ACS Catal* 2016;6:8115-20. DOI
68. Han N, Sun M, Zhou Y, et al. Alloyed palladium-silver nanowires enabling ultrastable carbon dioxide reduction to formate. *Adv Mater* 2021;33:e2005821. DOI
69. Sun Y, Wang F, Liu F, et al. Accelerating Pd electrocatalysis for CO_2-to-formate conversion across a wide potential window by optimized incorporation of Cu. *ACS Appl Mater Interfaces* 2022;14:8896-905. DOI
70. Chatterjee S, Griego C, Hart JL, et al. Free standing nanoporous palladium alloys as CO poisoning tolerant electrocatalysts for the electrochemical reduction of CO_2 to formate. *ACS Catal* 2019;9:5290-301. DOI
71. Guo S, Liu Y, Murphy E, et al. Robust palladium hydride catalyst for electrocatalytic formate formation with high CO tolerance. *Appl Catal B* 2022;316:121659. DOI
72. Jiang B, Zhang XG, Jiang K, Wu DY, Cai WB. Boosting formate production in electrocatalytic CO_2 reduction over wide potential window on Pd surfaces. *J Am Chem Soc* 2018;140:2880-9. DOI PubMed
73. Bok J, Lee SY, Lee BH, et al. Designing atomically dispersed Au on tensile-strained Pd for efficient CO_2 electroreduction to formate. *J Am Chem Soc* 2021;143:5386-95. DOI

74. Jia L, Sun M, Xu J, et al. Phase-dependent electrocatalytic CO_2 reduction on Pd_3 Bi nanocrystals. *Angew Chem Int Ed* 2021;60:21741-5. DOI
75. Ma J, Tan X, Zhang Q, Wang Y, Zhang J, Wang L. Exploring the size effect of Pt nanoparticles on the photocatalytic nonoxidative coupling of methane. *ACS Catal* 2021;11:3352-60. DOI
76. Yao Z, Yuan Y, Cheng T, et al. Anomalous size effect of Pt ultrathin nanowires on oxygen reduction reaction. *Nano Lett* 2021;21:9354-60. DOI
77. Cao Z, Kim D, Hong D, et al. A molecular surface functionalization approach to tuning nanoparticle electrocatalysts for carbon dioxide reduction. *J Am Chem Soc* 2016;138:8120-5. DOI
78. Dong C, Lian C, Hu S, et al. Size-dependent activity and selectivity of carbon dioxide photocatalytic reduction over platinum nanoparticles. *Nat Commun* 2018;9:1252. DOI PubMed PMC
79. Mayrhofer KJ, Blizanac BB, Arenz M, Stamenkovic VR, Ross PN, Markovic NM. The impact of geometric and surface electronic properties of pt-catalysts on the particle size effect in electrocatalysis. *J Phys Chem B* 2005;109:14433-40. DOI PubMed
80. Wu T, Han MY, Xu ZJ. Size effects of electrocatalysts: more than a variation of surface area. *ACS Nano* 2022;16:8531-9. DOI
81. Yang P, Li L, Zhao Z, Gong J. Reveal the nature of particle size effect for CO_2 reduction over Pd and Au. *Chin J Catal* 2021;42:817-23. DOI
82. Gao D, Zhou H, Wang J, et al. Size-dependent electrocatalytic reduction of CO_2 over Pd nanoparticles. *J Am Chem Soc* 2015;137:4288-91. DOI
83. Zhu W, Zhang L, Yang P, et al. Low-coordinated edge sites on ultrathin palladium nanosheets boost carbon dioxide electroreduction performance. *Angew Chem Int Ed* 2018;57:11544-8. DOI
84. Cao C, Xu Q, Zhu Q. Ultrathin two-dimensional metallenes for heterogeneous catalysis. *Chem Catal* 2022;2:693-723. DOI
85. Xu H, Shang H, Wang C, Du Y. Recent progress of ultrathin 2D Pd-based nanomaterials for fuel cell electrocatalysis. *Small* 2021;17:e2005092. DOI PubMed
86. Liu M, Pang Y, Zhang B, et al. Enhanced electrocatalytic CO_2 reduction via field-induced reagent concentration. *Nature* 2016;537:382-6. DOI
87. Zhang X, Zhang Z, Li H, et al. Insight into heterogeneous electrocatalyst design understanding for the reduction of carbon dioxide. *Adv Energy Mater* 2022;12:2201461. DOI
88. Xia Y, Xiong Y, Lim B, Skrabalak SE. Shape-controlled synthesis of metal nanocrystals: simple chemistry meets complex physics? *Angew Chem Int Ed* 2009;48:60-103. DOI PubMed PMC
89. Li F, Medvedeva XV, Medvedev JJ, et al. Interplay of electrochemical and electrical effects induces structural transformations in electrocatalysts. *Nat Catal* 2021;4:479-87. DOI
90. Xiao C, Lu B, Xue P, et al. High-index-facet- and high-surface-energy nanocrystals of metals and metal oxides as highly efficient catalysts. *Joule* 2020;4:2562-98. DOI
91. Tang Y, Chen Y, Wu Y, et al. High-indexed intermetallic Pt_3Sn nanozymes with high activity and specificity for sensitive immunoassay. *Nano Lett* 2023;23:267-75. DOI
92. Hall AS, Yoon Y, Wuttig A, Surendranath Y. Mesostructure-induced selectivity in CO_2 reduction catalysis. *J Am Chem Soc* 2015;137:14834-7. DOI PubMed
93. Liang J, Xia Y, Liu X, et al. Molybdenum-doped ordered $L1_0$ -PdZn nanosheets for enhanced oxygen reduction electrocatalysis. *SusMat* 2022;2:347-56. DOI
94. Gunji T, Ochiai H, Ohira T, Liu Y, Nakajima Y, Matsumoto F. Preparation of various Pd-based alloys for electrocatalytic CO_2 reduction reaction - selectivity depending on secondary elements. *Chem Mater* 2020;32:6855-63. DOI
95. Lu D, Fu X, Guo D, et al. Challenges and opportunities in 2D high-entropy alloy electrocatalysts for sustainable energy conversion. *SusMat* 2023;3:730-48. DOI
96. Yang S, Yang X, Cui X, et al. High C-C cleavage efficiencies of ethanol oxidation reaction on mesoporous RhPt electrocatalysts. *SusMat* 2022;2:689-98. DOI
97. Proietto F, Patel U, Galia A, Scialdone O. Electrochemical conversion of CO_2 to formic acid using a Sn based electrode: a critical review on the state-of-the-art technologies and their potential. *Electrochim Acta* 2021;389:138753. DOI
98. Gao N, Wang F, Ding J, et al. Intercalated gold nanoparticle in 2D palladium nanosheet avoiding CO poisoning for formate production under a wide potential window. *ACS Appl Mater Interfaces* 2022;14:10344-52. DOI
99. Kim D, Resasco J, Yu Y, Asiri AM, Yang P. Synergistic geometric and electronic effects for electrochemical reduction of carbon dioxide using gold-copper bimetallic nanoparticles. *Nat Commun* 2014;5:4948. DOI PubMed
100. Dong J, Cheng Y, Li Y, et al. Abundant (110) facets on $PdCu_3$ alloy promote electrochemical conversion of CO_2 to CO. *ACS Appl Mater Interfaces* 2022;14:41969-77. DOI
101. Bao K, Zhou Y, Wu J, et al. Super-branched PdCu alloy for efficiently converting carbon dioxide to carbon monoxide. *Nanomaterials* 2023;13:603. DOI PubMed PMC
102. Huang W, Wang Y, Liu J, et al. Efficient and selective CO_2 reduction to formate on Pd-doped $Pb_3(CO_3)_2(OH)_2$: dynamic catalyst reconstruction and accelerated CO_2 protonation. *Small* 2022;18:e2107885. DOI
103. Li H, Yue X, Qiu Y, et al. Selective electroreduction of CO_2 to formate over the co-electrodeposited Cu/Sn bimetallic catalyst. *Mater Today Energy* 2021;21:100797. DOI

104. Liu S, Wang X, Tao H, et al. Ultrathin 5-fold twinned sub-25 nm silver nanowires enable highly selective electroreduction of CO_2 to CO. *Nano Energy* 2018;45:456-62. DOI
105. Xie H, Wang T, Liang J, Li Q, Sun S. Cu-based nanocatalysts for electrochemical reduction of CO_2. *Nano Today* 2018;21:41-54. DOI
106. Chen Z, Liao Y, Chen S. Facile synthesis of platinum-copper aerogels for the oxygen reduction reaction. *Energy Mater* 2022;2:200033. DOI
107. Jiang T, Zhou Y, Ma X, et al. Spectrometric study of electrochemical CO_2 reduction on Pd and Pd-B electrodes. *ACS Catal* 2021;11:840-8. DOI
108. Wei K, Wang X, Ge J. PGM-free carbon-based catalysts for the electrocatalytic oxygen reduction reaction: active sites and activity enhancement. *Energy Mater* 2023:3. DOI
109. Liu S, Zhang H, Ren T, et al. Interface engineering and boron modification of Pd-B/Pd hetero-metallene synergistically accelerate oxygen reduction catalysis. *Small* 2023;19:e2306014. DOI
110. Lv H, Xu D, Sun L, et al. Ternary palladium-boron-phosphorus alloy mesoporous nanospheres for highly efficient electrocatalysis. *ACS Nano* 2019;13:12052-61. DOI
111. Jiang T, Yu L, Zhao Z, Wu W, Wang Z, Cheng N. Regulating the intermediate affinity on Pd nanoparticles through the control of inserted-B atoms for alkaline hydrogen evolution. *Chem Eng J* 2022;433:133525. DOI
112. Lin B, Wu X, Xie L, et al. Atomic imaging of subsurface interstitial hydrogen and insights into surface reactivity of palladium hydrides. *Angew Chem Int Ed* 2020;59:20348-52. DOI
113. Li H, Qin X, Zhang X, Jiang K, Cai W. Boron-doped platinum-group metals in electrocatalysis: a perspective. *ACS Catal* 2022;12:12750-64. DOI
114. Wang H, Li Y, Liu S, et al. B-doping-induced lattice expansion of Pd metallene nanoribbons for oxygen reduction reaction. *Inorg Chem* 2023;62:15157-63. DOI
115. Mao Z, Ding C, Liu X, et al. Interstitial B-doping in Pt lattice to upgrade oxygen electroreduction performance. *ACS Catal* 2022;12:8848-56. DOI
116. Shen T, Wang S, Zhao T, Hu Y, Wang D. Recent advances of single-atom-alloy for energy electrocatalysis. *Adv Energy Mater* 2022;12:2201823. DOI
117. Yang X, Wang Y, Tong X, Yang N. Strain engineering in electrocatalysts: fundamentals, progress, and perspectives. *Adv Energy Mater* 2022;12:2102261. DOI
118. Xia Z, Guo S. Strain engineering of metal-based nanomaterials for energy electrocatalysis. *Chem Soc Rev* 2019;48:3265-78. DOI PubMed
119. Jiang K, Zhang HX, Zou S, Cai WB. Electrocatalysis of formic acid on palladium and platinum surfaces: from fundamental mechanisms to fuel cell applications. *Phys Chem Chem Phys* 2014;16:20360-76. DOI PubMed
120. Shao Q, Wang P, Liu S, Huang X. Advanced engineering of core/shell nanostructures for electrochemical carbon dioxide reduction. *J Mater Chem A* 2019;7:20478-93. DOI
121. He T, Wang W, Shi F, et al. Mastering the surface strain of platinum catalysts for efficient electrocatalysis. *Nature* 2021;598:76-81. DOI
122. Luo M, Guo S. Strain-controlled electrocatalysis on multimetallic nanomaterials. *Nat Rev Mater* 2017;2:17059. DOI
123. Yan Y, Du JS, Gilroy KD, Yang D, Xia Y, Zhang H. Intermetallic nanocrystals: syntheses and catalytic applications. *Adv Mater* 2017;29:1605997. DOI PubMed
124. Li J, Sun S. Intermetallic nanoparticles: synthetic control and their enhanced electrocatalysis. *Acc Chem Res* 2019;52:2015-25. DOI PubMed
125. Zhou M, Li C, Fang J. Noble-metal based random alloy and intermetallic nanocrystals: syntheses and applications. *Chem Rev* 2021;121:736-95. DOI
126. Zeng Y, Liang J, Li C, et al. Regulating catalytic properties and thermal stability of Pt and PtCo intermetallic fuel-cell catalysts via strong coupling effects between single-metal site-rich carbon and Pt. *J Am Chem Soc* 2023;145:17643-55. DOI
127. Feng S, Geng Y, Liu H, Li H. Targeted intermetallic nanocatalysts for sustainable biomass and CO_2 valorization. *ACS Catal* 2022;12:14999-5020. DOI
128. Zhou F, Li H, Fournier M, MacFarlane DR. Electrocatalytic CO_2 reduction to formate at low overpotentials on electrodeposited Pd films: stabilized performance by suppression of CO formation. *ChemSusChem* 2017;10:1509-16. DOI
129. Hou Y, Erni R, Widmer R, et al. Synthesis and characterization of degradation-resistant Cu@CuPd nanowire catalysts for the efficient production of formate and CO from CO_2. *ChemElectroChem* 2019;6:3189-98. DOI
130. Yin Z, Yu J, Xie Z, et al. Hybrid catalyst coupling single-atom Ni and nanoscale Cu for efficient CO_2 electroreduction to ethylene. *J Am Chem Soc* 2022;144:20931-8. DOI
131. Kim D, Choi W, Lee HW, et al. Electrocatalytic reduction of low concentrations of CO_2 gas in a membrane electrode assembly electrolyzer. *ACS Energy Lett* 2021;6:3488-95. DOI
132. Ge L, Rabiee H, Li M, et al. Electrochemical CO_2 reduction in membrane-electrode assemblies. *Chem* 2022;8:663-92. DOI

133. Zhang Z, Huang X, Chen Z, et al. Membrane electrode assembly for electrocatalytic CO_2 reduction: principle and application. *Angew Chem Int Ed* 2023;62:e202302789. DOI

134. Dattila F, Seemakurthi RR, Zhou Y, López N. Modeling operando electrochemical CO_2 reduction. *Chem Rev* 2022;122:11085-130. DOI PubMed

135. Deng Y, Yeo BS. Characterization of electrocatalytic water splitting and CO_2 reduction reactions using in situ/operando raman spectroscopy. *ACS Catal* 2017;7:7873-89. DOI